Digital Comprehensive Summaries of Uppsala Dissertations
from the Faculty of Science and Technology 2388

Electrostatic turbulence and electron heating in collisionless shocks

AHMAD LALTI

ACTA UNIVERSITATIS
UPSALIENSIS
2024

ISSN 1651-6214
ISBN 978-91-513-2097-7
urn:nbn:se:uu:diva-526127

UPPSALA
UNIVERSITET

Dissertation presented at Uppsala University to be publicly examined in Heinz-Otto Kreiss, Å101195, Ångströmslaboratoriet, Lägerhyddsvägen 1, Uppsala, Friday, 31 May 2024 at 09:15 for the degree of Doctor of Philosophy. The examination will be conducted in English. Faculty examiner: Dr Christian Mazelle (Institut de Recherche en Astrophysique et Planétologie: Toulouse, Midi-Pyrénées, FR).

Abstract
Lalti, A. 2024. Electrostatic turbulence and electron heating in collisionless shocks. *Digital Comprehensive Summaries of Uppsala Dissertations from the Faculty of Science and Technology* 2388. 75 pp. Uppsala: Acta Universitatis Upsaliensis. ISBN 978-91-513-2097-7.

When the supersonic solar wind interacts with Earth's magnetosphere it forms a shock wave. However, due to the low densities in space, inter-particle collisions play an insignificant role in its dynamics. Earth's bow shock is an example of a collisionless shock, ubiquitous throughout the universe. Their dynamics are complex and their physics remains an active field of research. In this thesis, we use high-resolution measurements from NASA's Magnetospheric Multiscale (MMS) spacecraft to study the plasma wave activity across Earth's bow shock and its effects on electron heating. In Paper I we train a convolutional neural network (CNN) to identify the different plasma regions that MMS crosses. In Paper II we use the results of this CNN to compile a database of time intervals in which MMS crosses Earth's bow shock, which we use to find suitable events to tackle the science questions of interest. In Paper III we use multispacecraft methods to properly characterize obliquely propagating whistler waves running upstream of the shock. By analyzing the ion and electron distribution functions we find that their likely source is the instability between the incoming electrons and reflected ions. Shifting our focus to Debye scale electrostatic waves, in Paper IV we develop a method to measure their 3D wave vector based on single-spacecraft interferometry. We are in the process of using this method to study the evolution of Debye scale electrostatic waves across quasi-perpendicular shocks (see Chapter 7). Finally, in Paper V we investigate the electron heating mechanism across quasi-perpendicular shocks. We find the heating mechanism to depend on the Alfvénic Mach number in the deHoffman-Teller frame . We also find that at high the heating mechanism is consistent with the stochastic shock drift acceleration mechanism.

Keywords: Collisionless shocks, in-situ observations, plasma waves, wave-particle interaction, particle acceleration

Ahmad Lalti, Swedish Institute of Space Physics, Uppsala Division, Box 537, Uppsala University, SE-75121 Uppsala, Sweden. Department of Physics and Astronomy, Box 516, Uppsala University, SE-751 20 Uppsala, Sweden.

© Ahmad Lalti 2024

ISSN 1651-6214
ISBN 978-91-513-2097-7
URN urn:nbn:se:uu:diva-526127 (http://urn.kb.se/resolve?urn=urn:nbn:se:uu:diva-526127)

"Poets say science takes away from the beauty of the stars - mere globs of gas atoms. Nothing is "mere". I too can see the stars on a desert night, and feel them. But do I see less or more ?"

- Richard Feynman.

List of papers

This thesis is based on the following papers, which are referred to in the text by their Roman numerals.

I *Automated Classification of Plasma Regions Using 3D Particle Energy Distributions*
Olshevsky, V., Khotyaintsev, Y. V., **Lalti, A.**, Divin, A., Delzanno, G. L., Anderzén, S., Herman, P., Chien, S. W. D., Levon, A., Dimmock, A. P., Markidis, S.
Journal of Geophysical Research (Space Physics), vol. 126, no. 10, 2021.
doi:10.1029/2021JA029620.

II *A Database of MMS Bow Shock Crossings Compiled Using Machine Learning*
Lalti, A., Khotyaintsev, Y. V., Dimmock, A. P., Johlander, A., Graham, D. B., and Olshevsky, V.
Journal of Geophysical Research (Space Physics), vol. 127, no. 8, 2022.
doi:10.1029/2022JA030454.

III *Whistler Waves in the Foot of Quasi-Perpendicular Supercritical Shocks*
Lalti, A., Khotyaintsev, Y. V., Graham, D. B., Vaivads, A., Steinvall, K., and Russell, C. T.
Journal of Geophysical Research (Space Physics), vol. 127, no. 5, 2022.
doi:10.1029/2021JA029969.

IV *Short-Wavelength Electrostatic Wave Measurement Using MMS Spacecraft*
Lalti, A., Khotyaintsev, Y. V., and Graham, D. B.
Journal of Geophysical Research (Space Physics), vol. 128, no. 4, 2023.
doi:10.1029/2022JA031150.

V *Electron heating at quasi-perpendicular collisionless shocks*
Lalti, A., Khotyaintsev, Y. V., and Graham, D. B.
Manuscript submitted.

Reprints were made with permission from the publishers.

List of papers not included in this thesis

1. *Reinforced Shock Acceleration Uncovering the electron injection threshold*
   Raptis, S., **Lalti, A.**, Lindberg, M., Turner, D., Caprioli, C., Burch, J.
   Manuscript submitted.
2. *Ion Dynamics Across a Low Mach Number Shock*
   Graham, D. B., Khotyaintsev, Y. V., Dimmock, A. P., **Lalti, A.**, Boldú, J., Tigik, S., Fuselier, S.
   Journal of Geophysical Research (Space Physics), vol. 129, no. 4, 2024. doi:10.1029/2023JA032296.
3. *Backstreaming ions at a high Mach number interplanetary shock. Solar Orbiter measurements during the nominal mission phase*
   Dimmock, A. P., Gedalin, M., **Lalti, A.**, Trotta, D., Khotyaintsev, Yu. V., Graham, D. B., Johlander, A., Vainio R., Blanco-Cano X., Kajdič, P., Owen, C. J., Wimmer-Schweingruber, R. F.
   Astronomy and Astrophysics, vol. 679, 2023.
   doi:10.1051/0004-6361/202347006.
4. *Electron Heating Scales in Collisionless Shocks Measured by MMS*
   Johlander, A., Khotyaintsev, Y. V., Dimmock, A. P., Graham, D. B., and **Lalti, A.**
   Geophysical Research Letters, vol. 50, no. 5, 2023.
   doi:10.1029/2022GL100400.
5. *Analysis of multiscale structures at the quasi-perpendicular Venus bow shock. Results from Solar Orbiter's first Venus flyby*
   Dimmock, A. P., Khotyaintsev, Y. V., **Lalti, A.**, Yordanova, E., Edberg, N. J. T., Steinvall, K., Graham, D. B., Hadid, L. Z., Allen, R. C., Vaivads, A., Maksimovic, M., Bale, S. D., Chust, T., Krasnoselskikh, V., Kretzschmar, M., Lorfèvre, E., Plettemeier, D., Souček, J., Steller, M., Štverák, Š., Trávníček, P., Vecchio, A., Horbury, T. S., O'Brien, H., Evans, V., and Angelini, V.
   Astronomy and Astrophysics, vol. 660, 2022. doi:10.1051/0004-6361/202140954
6. *The spontaneous breaking of axisymmetry in shallow rotating flows*
   Antar, G., **Lalti, A.**, and Habchi, C.
   Physics of Fluids, vol. 31, no. 7, 2019. doi:10.1063/1.5098367

This PhD thesis is partly based on the licentiate dissertation "Electrostatic turbulence and electron heating in collisionless shocks" by Ahmad lalti, Uppsala University, 2022. Chapters have been edited and updated, and new material has been added.

Contents

1 Introduction 11

2 Collisonless shocks: a hierarchy of scales 14
2.1 The magnetohydrodynamic framework 14
2.1.1 The MHD equations 15
2.1.2 Linear waves in MHD 16
2.1.3 Non-linear waves in MHD: shock formation 18
2.1.4 The Rankin-Hugoniot conditions 20
2.2 The kinetic framework 21
2.3 Observations of collisionless shocks 24

3 Key parameters controlling shock dynamics 28
3.1 Mach numbers 28
3.2 Shock geometry 30

4 Particle dynamics at collisionless shocks 34
4.1 Ion dynamics 36
4.2 Electron dynamics 38
4.2.1 The adiabatic framework 38
4.2.2 The non-adiabatic framework 41

5 The Magnetospheric MultiScale mission 44
5.1 Particle distributions and moments 45
5.2 Electric field 46
5.3 Magnetic field 48
5.4 Multi and single spacecraft interferometry 48

6 Summary of papers 51
6.1 Paper I 51
6.2 Paper II 51
6.3 Paper III 52
6.4 Paper IV 53
6.5 Paper V 54

7 Outlook 55

8 Sammanfattning på svenska 59

9 Summary in Arabic 62

10 Acknowledgements 64

1. Introduction

When one pushes their hand into a pool of water, a force is exerted on the water molecules in contact with the hand causing them to move. In their motion, they will push on neighboring molecules, which in turn will move and push on their neighboring molecules, and so on. This initial local disturbance, caused by the hand, propagates away from the source in the form of compressional waves, called sound waves, and travels at the speed of sound in the medium. Sound waves occur for any object moving in any fluid (or any fluid flowing past any obstacle), they run ahead of the object, the hand in this case, and 'warn' the unperturbed fluid about what is to come. When the velocity of the object increases and exceeds the speed at which the sound waves propagate (i.e. it becomes supersonic), nothing can warn the fluid about what is coming, so it will be *shocked*. Subsequently, a shock wave will form ahead of the object.

Shock waves are a thin discontinuity, across which a supersonic flow is decelerated, and the excess kinetic energy is *irreversibly* transformed into heat. In media where inter-particle collisions are abundant, such as Earth's atmosphere, the heating is done through viscous dissipation driven by the collisions. Subsequently, the thickness of this discontinuity is of the same order as the average distance a particle travels between collisions, i.e. the mean free path of collisions in the medium λ_c. In our atmosphere, λ_c is of the order of nano-meters (10^{-9} m).

The study of shock waves in fluids was pioneered by Ernst Mach (Mach, 1898). Motivated by the science of bullets or fast projectiles, he hypothesized and experimentally verified that a shock wave forms when the velocity of the projectile surpasses the sound speed in the medium. In the following years, the field developed extensively especially due to its high relevance to military applications i.e. dynamics of bullets, bombs, and super-sonic fighter jets. It only took a few decades for the field to reach its maturity. Figure 1.1 shows in panel (a) the schematics of a shock wave around a supersonic bullet drawn by Mach, and panel (b) shows a modern high-resolution image of the same phenomena. Mach's schematics have the same features as the high-resolution image of a shock wave ahead of a bullet, with the shock wave and the turbulent downstream.

Fast forward 50 years, De Hoffmann and Teller, 1950 took on the interesting problem of studying shock waves in conducting fluids. In such fluids, long-distance interactions mediated by electric and magnetic fields, play a major role in the evolution of the system. Plasma, the fourth state of matter, is an example of a conducting fluid. It occurs when a gas is heated to the extent that

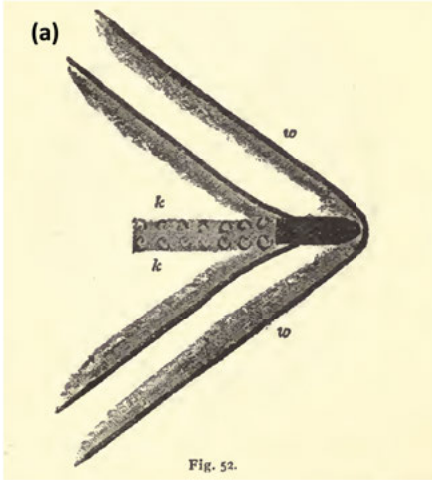

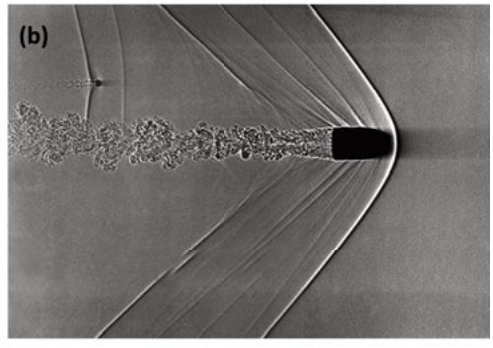

Figure 1.1. (a) Schematics of a shock wave around a bullet drawn by Ernst Mach from Mach, 1898, (b) Modern image of a shock wave around a supersonic bullet photographed using a shadowgraph, courtesy of Andrew Davidhazy/Rochester Institute of Technology.

electrons have enough energy to escape from the atom, so the gas is now comprised of floating negatively charged electrons and positively charged ions. Plasmas are not frequently encountered in our everyday life, yet it is believed that most of the visible matter in the universe, matter constituting galaxies, nebulae, and stars, are in the plasma state.

To describe the evolution of shock waves in conducting media, De Hoffmann and Teller used the framework of magneto-hydrodynamics (MHD). This framework uses the hydrodynamic equations and includes the force due to the electric and magnetic fields, i.e. the Lorentz force. Shock waves described by De Hoffmann and Teller sparked a huge interest in the scientific community. In addition to them being relevant to different astrophysical settings, they had a very peculiar property: they are collisionless. To simplify their calculations De Hoffmann and Teller assumed that the resistivity of the fluid is zero. The resistivity is a measure of how well the fluid conducts electric currents and is the macroscopic manifestation of the microscopic inter-particle collisions. So, in their calculations, De Hoffmann and Teller disregarded the effect of collisions on the evolution of the system.

Plasmas in space are highly tenuous and span vast distances. The solar wind for example, the continuous supersonic stream of plasma emanating from the Sun, has a density of ~ 10 particles in each cubic centimeter[1], at 1 Astronomical Unit (AU)[2]. In comparison, the density of the air we breathe is $\sim 10^{19}$

[1] Each cubic centimeter, cm^3, is one-fifth of a teaspoon in volume.
[2] 1 AU is roughly the distance from the earth to the sun $\sim 1.5 \cdot 10^8$ km.

particles per cubic centimeter[3]. When this supersonic flow hits an obstacle, such as a planet, it will form a plasma shock wave similar to that described by De Hoffmann and Teller. An example of such a phenomenon is Earth's bow shock, observed for the first time using in situ observations by Ness et al., 1964. At the low densities of the solar wind, the collisional mean free path is around 5 AU or $7.5 \cdot 10^8$ km, which is orders of magnitude larger than the whole magnetic environment around Earth (called the Magnetosphere) approximately at $6 \cdot 10^6$ km. For such shock waves, collisions do not play any role in their dynamics; they are collisionless.

But shocks without collisions seem like an oxymoron! A key feature of a shock wave is that it irreversibly dissipates energy across it, usually through inter-particle collisions. So, if collisions are non-existent: what else could play this defining role in the dynamics of shocks in space plasmas? This question motivated many publications, the most seminal of which is that of Sagdeev, 1966 who predicted that the interaction between charged particles in the plasma with oscillations in the magnetic and electric fields could play the role of collisions. Under certain conditions[4], charged particles can exchange energy with the various waves excited in the plasma, either gaining energy from or feeding energy to the waves. This wave-particle interaction generates some form of 'anomalous' resistivity that could irreversibly dissipate energy and sustain a shock wave in collisionless media. This result was the cornerstone for the development of the physics of collisionless shocks, a field that extends in importance to all sectors of the universe, and to this day is a highly active field of research.

In this thesis, I present my contributions to two of the remaining open questions on the physics of collisionless shocks, namely, the questions of *Electrostatic turbulence* and *electron heating* in collisionless shocks[5]. The thesis is structured as follows: Chapter 2 will give a general non-extensive[6] overview of the physics of collisionless shocks along with an overview of Earth's bow shock, the main laboratory that I used to conduct my research. Chapter 3 introduces key parameters controlling the dynamics of the shock. Chapter 4 will describe how ions and electrons behave as they cross the shock. Chapter 5 will introduce the spacecraft along with its various instruments used to investigate the questions of interest. Chapter 6 summarizes the main techniques employed and results obtained in each of the papers included in this thesis. Chapter 7 lists some preliminary results of ongoing research and possible remaining open questions for future investigation. Summaries in Swedish and Arabic can be found in Chapters 8 and 9 respectively.

[3]That's 1 with 19 zeros next to it!

[4]The resonance conditions.

[5]And hence the title of this thesis.

[6]For more detailed accounts on the subject many references can be consulted such as Tidman and Krall, 1971, Kennel et al., 1985, Balogh and Treumann, 2013, and Burgess and Scholer, 2015 to name a few.

2. Collisonless shocks: a hierarchy of scales

The most detailed classical description of a many-body system is to write down its full Hamiltonian, including every degree of freedom in the system with a potential that captures the internal interaction of the system along with any external forces. Such an exercise is useful for a simple system where one can obtain an analytic solution or for a non-integrable system with a small enough number of degrees of freedom that one can solve the equations computationally in a reasonable amount of time. But as the number of degrees of freedom increases this task becomes more and more tedious even for the most advanced supercomputers. So physicists do what they do best, they break down the system into a hierarchy of scales and then coarse-grain the equations to an extent that a solution can be obtained. At the largest level of coarse-graining, one looks at a global description of the system with disregard to any small-scale effects. Although information will be lost, the coarse-grained system can still be highly valuable to understanding the dynamics and evolution of the actual system. Then, the physicist would add layers of complexity, and relax simplifying assumptions gradually until a reasonable picture of the behavior and dynamics of the actual system is reached.

In this Chapter, an outline of the most and least coarse-grained descriptions of collisionless shocks are given in Sections 2.1 and 2.2 respectively. The theoretical description of collisionless shocks has to be backed by experimental and observational proofs. Section 2.3 gives an overview of observations of collisionless shocks in the Universe, with emphasis on the most studied collisionless shock: Earth's bow shock.

2.1 The magnetohydrodynamic framework

The most coarse-grained description of a plasma is within the framework of magnetohydrodynamics (MHD). In this framework, the system is described by: the set of conservation equations (mass, momentum, and energy) coupled with Maxwell's equations for the electric and magnetic fields, along with a generalized Ohm's law and an equation of state. The electrons and ions dynamics are lumped together, and the plasma is considered as a single fluid that evolves under the effect of the Lorentz force. Any term in the equations that is of the order of the electron mass is neglected and quasi-neutrality is assumed.

2.1.1 The MHD equations

In what follows, I present, without deriving them, the equations describing the dynamics of a plasma in the MHD regime (the equations can be found in any textbook on plasma physics, I take the results from Baumjohann and Treumann, 2012).
Conservation of mass:

$$\frac{\partial n}{\partial t} + \nabla \cdot (n\mathbf{v}) = 0, \tag{2.1}$$

conservation of momentum:

$$\frac{\partial (nm\mathbf{v})}{\partial t} + \nabla \cdot (nm\mathbf{v}\mathbf{v}) = -\nabla \cdot \mathbf{P} + \rho\mathbf{E} + \mathbf{j} \times \mathbf{B}, \tag{2.2}$$

conservation of energy:

$$\frac{\partial}{\partial t}\left[nm\left(\frac{v^2}{2} + w\right) + \frac{B^2}{2\mu_0}\right] = -\nabla \cdot \mathbf{q}, \tag{2.3}$$

where $\mathbf{q}$ is the heat flux density vector given by:

$$\mathbf{q} = nm\mathbf{v}\left(\frac{v^2}{2} + w + \frac{p + B^2/\mu_0}{nm}\right) - \frac{\mathbf{B}}{\mu_0}\left(\mathbf{v} + \frac{\mathbf{j}}{ne}\right) \cdot \mathbf{B} - \frac{\eta \mathbf{j} \times \mathbf{B}}{\mu_0} + \frac{\mathbf{j}B^2}{\mu_0 ne} + \frac{m_e \mathbf{B}}{\mu_0 ne^2} \times \frac{\partial \mathbf{j}}{\partial t}. \tag{2.4}$$

In the above equations

$$n = \frac{\sum m_s n_s}{\sum m_s}, \tag{2.5}$$

is the density of the plasma if considered as a single fluid, with n_s and m_s being the density and mass of species s either e for electrons or i for ions.

$$m = \sum m_s, \tag{2.6}$$

is the single fluid mass,

$$\mathbf{v} = \frac{\sum m_s n_s \mathbf{v}_s}{\sum m_s n_s}, \tag{2.7}$$

is the single fluid velocity. Furthermore, $\rho = \sum e_s n_s$ and $\mathbf{j} = \sum e_s n_s \mathbf{v}_s$ are the charge and current densities respectively, $\mathbf{E}$ and $\mathbf{B}$ are the electric and magnetic fields respectively, $\mathbf{P}$ is the pressure tensor of the single fluid, η represents the resistivity of the system, p is the isotropic pressure, and w is the enthalpy.

For the fields, Maxwell's equations are:

$$\nabla \times \mathbf{B} = \mu_0 \mathbf{j} + \mu_0 \varepsilon_0 \frac{\partial \mathbf{E}}{\partial t}, \tag{2.8}$$

$$\nabla \times \mathbf{E} = -\frac{\partial \mathbf{B}}{\partial t}, \tag{2.9}$$

$$\nabla \cdot \mathbf{B} = 0, \tag{2.10}$$

and

$$\nabla \cdot \mathbf{E} = \frac{\rho}{\varepsilon_0}, \tag{2.11}$$

with μ_0 and ε_0 being the permeability and permittivity of free space. The generalized Ohm's law gives a relation between the current density $\mathbf{j}$ and the electric field $\mathbf{E}$:

$$\mathbf{E} + \mathbf{v} \times \mathbf{B} = \eta \mathbf{j} + \frac{\mathbf{j} \times \mathbf{B}}{ne} - \frac{\nabla \cdot \mathbf{P}_e}{ne} + \frac{m_e}{ne^2} \frac{\partial \mathbf{j}}{\partial t}. \tag{2.12}$$

Finally to close the system of equations one requires the appropriate equation of state which is an empirical relation between the pressure, temperature, and density in the fluid.

The above equations represent a set of non-linear coupled differential equations describing the full dynamics of a single conducting fluid. To further simplify the equations (additional course-graining), one can assume, as De Hoffmann and Teller did, that the fluid is infinitely conductive, which means the resistivity η is zero. In addition, under certain conditions, most of the right-hand side terms in Equation 2.12 are very small compared to the left-hand side terms. Under such assumptions Equation 2.12 reduces to:

$$\mathbf{E} = -\mathbf{v} \times \mathbf{B}. \tag{2.13}$$

The physical implication of those assumptions is that the magnetic field cannot move freely in the fluid anymore. If the magnetic field were to drift, according to Faraday's law (Eq. 2.9), its time dependence would induce an electric field in the plasma. Since the resistivity is assumed to vanish, the plasma will directly move to short-circuit this electric field and counterbalance any change in the magnetic field. This has the effect that the magnetic field lines are stuck to the plasma as it moves, it is said to be *frozen* into it.

2.1.2 Linear waves in MHD

A plasma in the MHD regime, where both the velocity $\mathbf{v}$ and the electric field $\mathbf{E}$ are zero is in a state of equilibrium. This is the state where the system is steady (all quantities do not depend on time) and is in an overall pressure balance. If this equilibrium is perturbed, various waves can be excited, called the normal modes of the system. Using perturbation theory, one can find the characteristics of those waves.

Let f stand for any fluid variable (velocity, magnetic field, pressure, etc...). At equilibrium, $f = f_0$ satisfies the MHD equations. To perturb the system, f is assumed to be equal to $f_0 + \delta f$ with δf being a small perturbation. Replacing in the MHD Equations 2.1 - 2.3, 2.8 - 2.11, 2.13, and keeping terms

that are of the first order in δf, one obtains the linearized MHD equations (not shown).

A general solution of the linear equations is that of a plane wave of the form $\delta f = \delta \tilde{f} \exp i(\mathbf{k}\cdot\mathbf{x} - \omega t)$. $\delta \tilde{f}$ is the complex amplitude of the disturbance, $\mathbf{k}$ is the wave normal vector, the vector pointing in the direction normal to the wavefront and with a magnitude $2\pi/\lambda$ with λ being the wavelength of the wave, and ω is the angular frequency of the wave. This will transform the set of partial differential equations into a set of algebraic equations that can be easily solved. If one replaces all variables by their dependence on the velocity fluctuation $\delta\mathbf{v}$, the following matrix equation is obtained:

$$\begin{bmatrix} \omega^2 - v_A^2 k^2 \cos^2(\theta_{kB}) - c_{ms}^2 k^2 \sin^2(\theta_{kB}) & 0 & -c_s^2 k^2 \sin(\theta_{kB})\cos(\theta_{kB}) \\ 0 & \omega^2 - v_A^2 k^2 \cos^2(\theta_{kB}) & 0 \\ -c_s^2 k^2 \sin(\theta_{kB})\cos(\theta_{kB}) & 0 & \omega^2 - c_s^2 k^2 \cos^2(\theta_{kB}) \end{bmatrix} \cdot \begin{bmatrix} \delta v_{0x} \\ \delta v_{0y} \\ \delta v_{0x} \end{bmatrix} = 0., \tag{2.14}$$

where $v_A = \sqrt{\frac{B^2}{\mu_0 n m_i}}$ is the Alfvén speed, $c_s = \sqrt{\gamma p_0 / m_i n_0}$ is the sound speed with γ the heat capacity ratio, $c_{ms} = \sqrt{c_s^2 + v_A^2}$ is the magnetosonic speed and θ_{kB} is the angle between the wave normal vector $\mathbf{k}$ and the background magnetic field $\mathbf{B}_0$.

For this equation to have a non-trivial solution the determinant of the matrix multiplying $\delta\mathbf{v}$ should be equal to zero. This will give us a polynomial in ω whose roots are the dispersion relations[1] of the normal modes of the system.

Following this analysis, one finds three different wave modes that can be excited in an MHD plasma: the shear Alfvén wave with dispersion relation:

$$\omega_A^2 = k^2 v_A^2 \cos^2(\theta_{kB}), \tag{2.15}$$

and the fast and slow magnetosonic waves with dispersion relation:

$$\omega_{ms}^2 = \frac{k^2}{2}\left\{ c_{ms}^2 \pm \left[\left(v_A^2 - c_s^2\right)^2 + 4 v_A^2 c_s^2 \sin^2(\theta_{kB}) \right]^{(1/2)} \right\}. \tag{2.16}$$

Dividing equations 2.15 and 2.16 by k^2 then taking the square root, one obtains the phase speed, $v_{ph} = \omega/k$, for each mode[2]. The largest of the two speeds coming from Equation 2.16 corresponds to the fast mode c_f and the smallest corresponds to the slow mode c_{sl} with $c_f \geq v_A \geq c_{sl}$.

In this description of a plasma, three different wave modes can transport information from one place to another, compared to only one (the sound wave) in regular hydrodynamics. Also, in contrast to sound waves in hydrodynamics, the phase speed of those MHD waves is dependent on the angle between the wave vector and the background magnetic field. Figure 2.1 shows the polar

[1] The dispersion relation describes the variation of the frequency of the wave with the variation of its wavenumber.

[2] The phase speed $= \omega/k$ is the speed of propagation of a single frequency component of a wave packet at a constant phase.

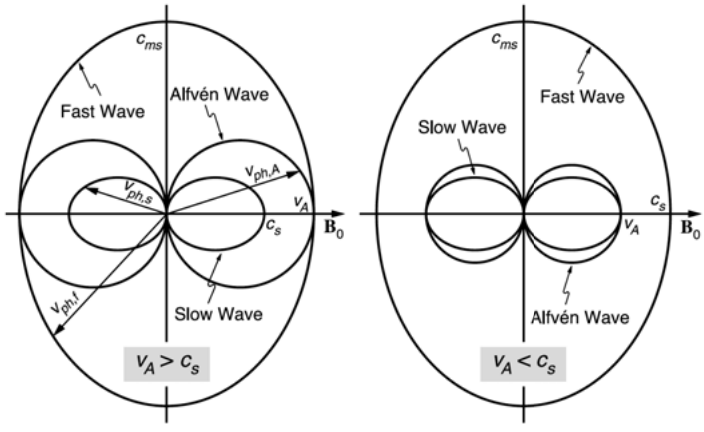

Figure 2.1. Polar plots of the phase velocity, called the wave normal surfaces, for the three MHD waves. The x and y axis represent the directions parallel and perpendicular to the background magnetic field respectively, the contours represent the magnitude of the phase speed, while the angle that the vector makes with respect to the x-axis (the polar angle) is θ_{kB}. The plot on the left (right) is for the case when v_A is larger (smaller) than c_s. Reprinted with permission from Balogh and Treumann, 2013

.

plot of the phase velocity, called the wave normal surface where the x and y axes represent the directions parallel and perpendicular to the background magnetic field respectively. The contours represent the magnitude of the phase speed, while the angle that the vector makes with respect to the x-axis (the polar angle) is θ_{kB}. Only the fast mode wave can propagate perpendicular to **B**, and all three modes can propagate at all other angles.

If plasma flows at a velocity larger than any of the three phase velocities, three different types of shock waves can form when the flow encounters an obstacle: fast, intermediate, and slow shocks. For the slow and intermediate shocks to form there have to be special conditions in the plasma preventing the other faster modes from propagating. Therefore, the most abundant of the three is the fast mode shock waves.

2.1.3 Non-linear waves in MHD: shock formation

When energy is injected into the system, the amplitude of the linear waves described earlier will tend to grow and the linear description (assuming a solution of the form $f = f_0 + \delta f$, and keeping only terms that are linear in δf) will not hold anymore. Non-linear interaction will become more and more dominant, which will cause coupling of the scales together, i.e. larger wavelength waves will excite smaller wavelength waves. The free energy input to

the system will cascade into smaller and smaller scales, causing the amplitude of the short wavelength wave to grow, and the wave to steepen. This non-linear steepening will reach a threshold beyond which the wave experiences a gradient catastrophe and starts to break on itself (Krasnoselskikh et al., 2002) just like ocean waves (see Figure 2.2).

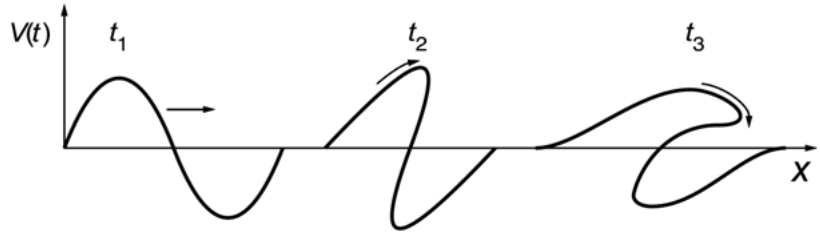

Figure 2.2. Schematics of wave steepening and breaking at three different stages of its evolution: linear (left), non-linearly steepened (middle), and breaking (right). Reprinted with permission from Balogh and Treumann, 2013.

The gradient catastrophe and the breaking of the wave can be prevented if at a certain scale length energy is removed from the system. Two different mechanisms can do the job: dispersion and dissipation.

Dispersion occurs when smaller wavelength waves have different group speed[3] than larger wavelength waves. In such a case small-scale waves generated by the non-linear cascade will either outrun or trail behind the main structure. In this process, energy is removed from the system, balancing the non-linear steepening. This is represented schematically in Figure 2.3. On the left, two dispersion curves (ω vs k) are plotted one is convex and the other concave. The former, contrary to the latter, will have a larger group speed at a smaller wavelength. On the right of Figure 2.3, the top and bottom panels represent how a steepening wave will have a trailing and a precursor wave train corresponding to the concave and convex dispersion relations respectively. The waves derived from MHD are non-dispersive, or the group speed is independent of wavelength. When the MHD framework is not valid anymore one requires a more complex description of the plasma such as the two fluids or the kinetic descriptions. For those descriptions, the waves become dispersive, opening up the possibility for dispersion to balance the non-linear steepening, and creating a stable structure.

A defining feature of a shock wave is the irreversible dissipation of energy and the generation of entropy across it. So, dispersively balanced non-linear waves are stable, yet they cannot be called shock waves, since the process of dispersion is reversible.

[3]The group speed $= \frac{\partial \omega}{\partial k}$, is the speed of propagation of the envelope of the wave packet (it corresponds to the speed of transport of energy).

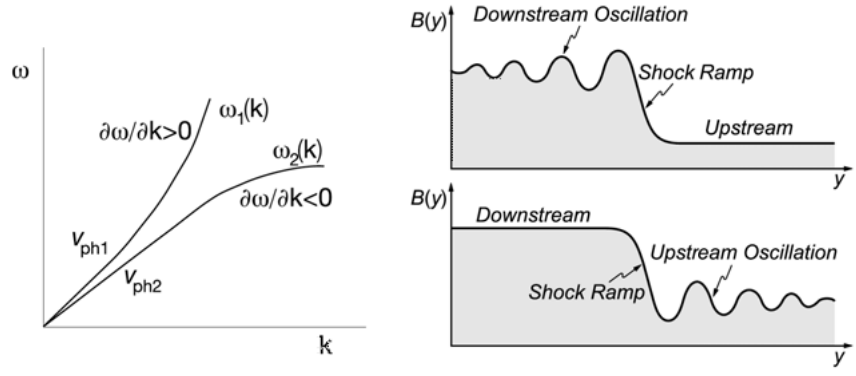

Figure 2.3. Schematics of wave dispersion at a non-linearly steepening plasma wave. The left represents two convex and concave dispersion relations. The right represents a trailing (top) and a precursor (bottom) wave train at a non-linearly steepening structure. Reprinted with permission from Balogh and Treumann, 2013.

Through dissipation, energy is irreversibly lost from the system. When dissipation exists, the non-linear steepening can be balanced, and the stable structure that results can be called a shock. Even though the plasma is collisionless, at a certain scale length, the interaction between particles and fields will become strong enough to play the role of collisions and generate *anomalous* dissipation in the system (more on this in the next section).

2.1.4 The Rankin-Hugoniot conditions

The magnetohydrodynamic description of a collisionless shock does not include the details of the physics occurring inside the ramp. In this description, the shock is treated as a black box, a very thin discontinuity across which the conservation laws are obeyed. Using those conservation equations one can predict the downstream plasma parameters (such as magnetic field, velocity, density, etc...) given their upstream values. This is done by assuming all changes of the plasma parameters occur exactly at the ramp, so one can ignore all gradients tangent to the shock compared to those along its normal direction $\hat{\mathbf{n}}$. So, all gradients in the equations describing the flow can be replaced by $\hat{\mathbf{n}}\frac{\partial}{\partial n}$. Furthermore, since the width of the shock is assumed small compared with the scale of the system, the derivative can be approximated by a difference in the following way

$$\nabla X \rightarrow \hat{\mathbf{n}}\frac{\partial}{\partial n} \rightarrow \hat{\mathbf{n}}\frac{[X]}{\delta}. \tag{2.17}$$

Where X is any parameter, $[X] = X_2 - X_1$ is the change in that parameter across the shock, and δ is the shock width. One could apply this to the conservation

laws of the MHD equations and integrate them to get a set of algebraic equations relating the plasma and field parameters upstream and downstream of the shock. Those are called the Rankine-Hugoniot jump conditions across the shock and they read (Baumjohann and Treumann, 2012):

$$\hat{\mathbf{n}} \cdot [n\mathbf{v}] = 0, \tag{2.18}$$

$$\hat{\mathbf{n}} \cdot [nm\mathbf{v}\mathbf{v}] + \hat{\mathbf{n}} \left[p + \frac{B^2}{2\mu_0} \right] - \frac{\hat{\mathbf{n}} \cdot [\mathbf{B}\mathbf{B}]}{\mu_0} = 0, \tag{2.19}$$

$$\hat{\mathbf{n}} \times [\mathbf{v} \times \mathbf{B}] = 0, \tag{2.20}$$

$$\hat{\mathbf{n}} \cdot [\mathbf{B}] = 0, \tag{2.21}$$

$$nm\hat{\mathbf{n}} \cdot \mathbf{v} \left[\frac{v^2}{2} + w + \frac{1}{nm} \left(p + \frac{B^2}{\mu_0} \right) \right] - \frac{1}{\mu_0} (\mathbf{v} \cdot \mathbf{B}) \hat{\mathbf{n}} \cdot \mathbf{B} = 0. \tag{2.22}$$

Multiple solutions exist for the above set of algebraic equations, each corresponding to a different class of discontinuity, rotational or tangential discontinuity, and of course all three types of shocks (fast, intermediate, and slow).

A fast mode shock, the discontinuity of interest in this thesis, is characterized by a constant non-vanishing normal flux of plasma across the discontinuity $nv_n \neq 0$, an increase in the plasma pressure $[p] > 0$, temperature $[T] > 0$, density $[n] > 0$, and magnetic pressure $\left[B_t^2\right] > 0$, with B_t being the magnetic field component tangent to the shock.

A very important corollary of the Rankine-Hugoniot jump condition is the coplanarity theorem. One can show, using the Rankine-Hugoniot jump conditions, that across fast collisionless shocks, the upstream and downstream magnetic fields fall in the same plane as the shock normal. The same result can be obtained with the upstream and downstream flow velocities.

2.2 The kinetic framework

One of the least coarse-grained descriptions of a plasma is the kinetic description. The Hamiltonian of a system of N interacting particles is:

$$\mathscr{H} = \sum_{\alpha=0}^{N} \frac{p_\alpha^2}{2m_\alpha} + \mathscr{V}(\mathbf{p}_\alpha, \mathbf{q}_\alpha), \tag{2.23}$$

where $\mathbf{p}_\alpha$ and $\mathbf{q}_\alpha$ are the generalized coordinate and momentum of particle α, and $\mathscr{V}$ is the total potential containing contributions from external forces and the interactions between the particles. The solution for this system represents a trajectory followed by a single point in the 6N dimensional phase space (3N coordinates and 3N momenta), along which the energy is conserved $\frac{d\mathscr{H}}{dt} = 0$. Instead of looking at a single trajectory, one can look at the statistical distribution of the different points in phase space pertaining to different trajectories

obtained by varying the initial conditions of the system. One would obtain the N particle probability distribution function $F_N(\mathbf{q}_1,...,\mathbf{q}_\alpha,\mathbf{p}_1,...,\mathbf{p})$ in the 6N dimensional phase space. According to Liouville's theorem, this distribution function is conserved along trajectories in phase space, so:

$$\frac{dF_N}{dt} = \frac{\partial F_N}{\partial t} + \{F_N;\mathscr{H}\} = 0, \tag{2.24}$$

Where $\{F_N;\mathscr{H}\}$ is the Poisson bracket between F_N and $\mathscr{H}$ defined as:

$$\{F_N;\mathscr{H}\} = \sum_{\alpha=0}^{N}\left[\frac{\partial F_N}{\partial \mathbf{q}_\alpha}\cdot\frac{\partial \mathscr{H}}{\partial \mathbf{p}_\alpha} - \frac{\partial F_N}{\partial \mathbf{p}_\alpha}\cdot\frac{\partial \mathscr{H}}{\partial \mathbf{q}_\alpha}\right]. \tag{2.25}$$

Solving equation 2.24 would amount to solving for the full dynamics of the system under any initial condition. But as mentioned at the beginning of this chapter, this task is nearly impossible when N becomes large, so physicists devised different ways to go around this problem. One of which is the BBGKY Theory named after the initials of the scientists who devised it, where equation 2.24 is integrated along multiple degrees of freedom to get a reduced distribution whose equation is easier to deal with. The details of the theory, although interesting, are mathematically involved and are outside the scope of this thesis. The interested reader is referred to Montgomery and Tidman, 1964.

For a collisionless plasma, one can integrate over all but one of the degrees of freedom, obtaining the single-particle distribution function $f_s(\mathbf{p},\mathbf{q})$, for each species s in the plasma, which is also conserved along phase space trajectories. If we take into consideration that the only source of interaction is through the Lorentz force, equation 2.24 reduces to:

$$\frac{\partial f_s}{\partial t} + \mathbf{v}\cdot\nabla f_s + \frac{e_s}{m_s}(\mathbf{E}+\mathbf{v}\times\mathbf{B})\cdot\nabla_{\mathbf{v}} f_s = 0, \tag{2.26}$$

where $\nabla_{\mathbf{v}}$ is the gradient with respect to the velocity coordinate in phase space and e_s and m_s are the electric charge and mass of the species s. The electric and magnetic fields are determined from Maxwell's equations (equations 2.8-2.10), with the charge and current densities written as:

$$\mathbf{j} = \sum_s e_s \int \mathbf{v} f_s d\mathbf{v}, \tag{2.27}$$

and

$$\rho = \sum_s e_s \int f_s d\mathbf{v}. \tag{2.28}$$

This system of equations is called the Vlasov equations, which can describe the dynamics of complex phenomena in collisionless plasmas down to the smallest scales. Naturally, a lot could be explored about collisionless shocks

by using a kinetic theoretic approach, yet the equations are still not fully solvable analytically. Therefore, to get any theoretical knowledge out of these equations one must resort to further simplifying assumptions, or to kinetic numerical simulations.

To carry on from the last section, and to show the power of the kinetic description, one can use the above kinetic equations to understand how irreversible dissipation could arise in a collisionless plasma. To do so it is assumed that the distribution function for each species f_s is comprised of an averaged term $f_{s0} = \langle f_s \rangle$ plus a fluctuation term δf_s, i.e. $f_s = f_{s0} + \delta f_s$. The fluctuations in the distribution function have the property that $\langle \delta f_s \rangle = 0$. By using the same approximation for the fields and plugging everything into the Vlasov equations, one obtains two equations one for the averaged quantities (denoted with the subscript 0):

$$\frac{\partial f_{s0}}{\partial t} + \mathbf{v} \cdot \nabla f_{s0} + \frac{e_s}{m_s} (\mathbf{E_0} + \mathbf{v} \times \mathbf{B}_0) \cdot \nabla_{\mathbf{v}} f_{s0} = -\frac{e_s}{m_s} \langle (\delta \mathbf{E} + \mathbf{v} \times \delta \mathbf{B}) \cdot \nabla_{\mathbf{v}} \delta f_s \rangle, \tag{2.29}$$

and one for the fluctuations:

$$\begin{aligned} \frac{\partial \delta f_s}{\partial t} + \mathbf{v} \cdot \nabla \delta f_0 + \frac{e_s}{m_s} (\mathbf{E_0} + \mathbf{v} \times \mathbf{B}_0) \cdot \nabla_{\mathbf{v}} \delta f_s = -\frac{e_s}{m_s} (\delta \mathbf{E} + \mathbf{v} \times \delta \mathbf{B}) \cdot \nabla_{\mathbf{v}} f_{s0} \\ - \frac{e_s}{m_s} (\delta \mathbf{E} + \mathbf{v} \times \delta \mathbf{B}) \cdot \nabla_{\mathbf{v}} \delta f_s + \frac{e_s}{m_s} \langle (\delta \mathbf{E} + \mathbf{v} \times \delta \mathbf{B}) \cdot \nabla_{\mathbf{v}} \delta f_s \rangle, \end{aligned} \tag{2.30}$$

The last term in both equations contains the averages of the multiplication of two fluctuating quantities, which do not necessarily vanish. This term represents the anomalous dissipation in collisionless shocks. Physically it comes from the interactions between the oscillating fields and the charged particles. When the particles and the waves are in resonance, they can exchange energy, which will affect the dynamics of the particles. On average, this interaction can irreversibly change the bulk kinetic energy of the particles into randomized thermal energy across the shock and play the role of collisions. An estimate of the anomalous collision frequency ν is given by:

$$\nu \simeq \frac{W_{sat}}{N T_e} \omega_{pe}, \tag{2.31}$$

with W_{sat} is the saturation energy of the wave, N the density, T_e the electron temperature, and ω_{pe} the electron plasma frequency. Many wave modes can efficiently generate anomalous dissipation, such as ion or electron acoustic waves, electron cyclotron drift instability waves, and lower hybrid drift instability waves, to name a few. Many of those wave modes have been observed across collisionless shocks reaching high amplitudes with the highest electric field amplitude measured in the near-Earth environment, in Chapter 4, examples of such waves from spacecraft measurement, along with discussion regarding their interplay with the particles will be presented.

2.3 Observations of collisionless shocks

The previous sections focused on the theoretical development of the physics of collisionless shocks. But the theory has been shaped, as the scientific method requires, by observational evidence. Observation of collisionless shocks was first achieved in a laboratory experiment in 1965 by Kurtmullaev et al., 1965, but the most conclusive evidence for their existence was when the IMP 1 spacecraft crossed the bow shock around Earth and measured the magnetic field jump across the shock (Ness et al., 1964). Figure 2.4 shows one of the first observations of a shock crossing. On January 20, 1964, IMP 1 was initially in the magnetosphere, it crossed the magnetopause at around 21:00 then the bow shock at around 05:45 on January 21, 1964. After that, and with

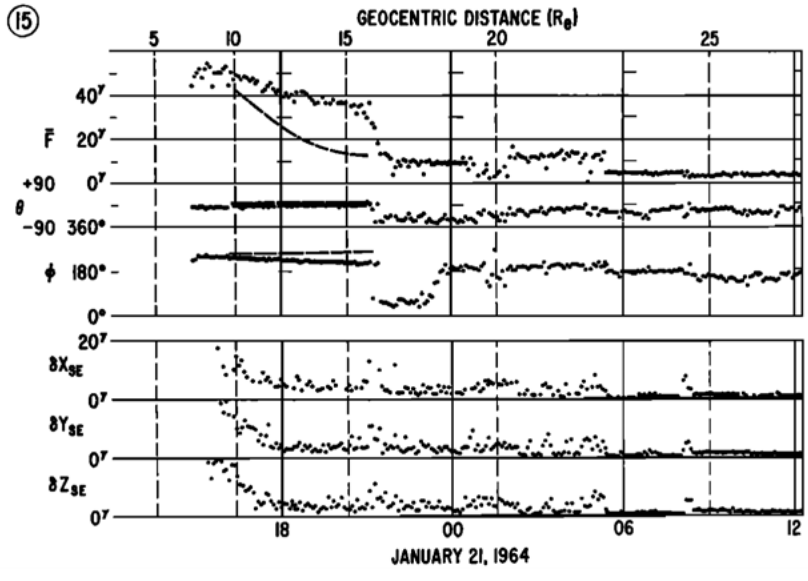

Figure 2.4. Magnetic field data from the IMP 1 spacecraft showing one of the first crossings of the magnetopause and Earth's bow shock. Reprinted with permission from Ness et al., 1964

the booming of the space age, many spacecraft were sent all across the heliosphere, many of which observed collisionless shocks. From Inter-Planetary (IP) shocks [4] observed by ACE (Stone et al., 1998), Wind (Harten and Clark, 1995) and the most recent Solar Orbiter (Müller et al., 2020) spacecraft, to bow shocks around different planets such as Saturn using Cassini (Sulaiman et al., 2016) and at Venus using Venus Express (Zhang et al., 2008). The far-

[4] IP shocks form when a fast solar wind stream overtakes a slow solar wind stream. It usually occurs ahead of coronal mass ejections (CMEs) or stream interaction regions (SIRs).

thest shock from Earth observed in situ is the termination shock[5], crossed by the Voyager 1 and 2 spacecraft (Li et al., 2008).

Astrophysical collisionless shocks, outside the heliosphere, are only accessible through remote sensing. Shocks at supernova remnants (SNR) or active galactic nuclei (AGN) can reach relativistic speeds and are believed to be the primary source of cosmic rays (Blasi, 2013; Bykov and Treumann, 2011). The existence of such shocks, along with their properties, have been inferred from the observed electromagnetic (X-rays and γ-Rays) emissions coming from the shock. An example is seen in Figure 2.5, showing an image of the Tycho SNR taken by the Chandra X-Ray observatory. The red signature is coming from the ejecta of the supernova. The blue halo around the SNR is the signature of the shock forming between the supersonic ejecta and the interstellar medium. This halo is due to the synchrotron radiation from accelerated electrons at the shock.

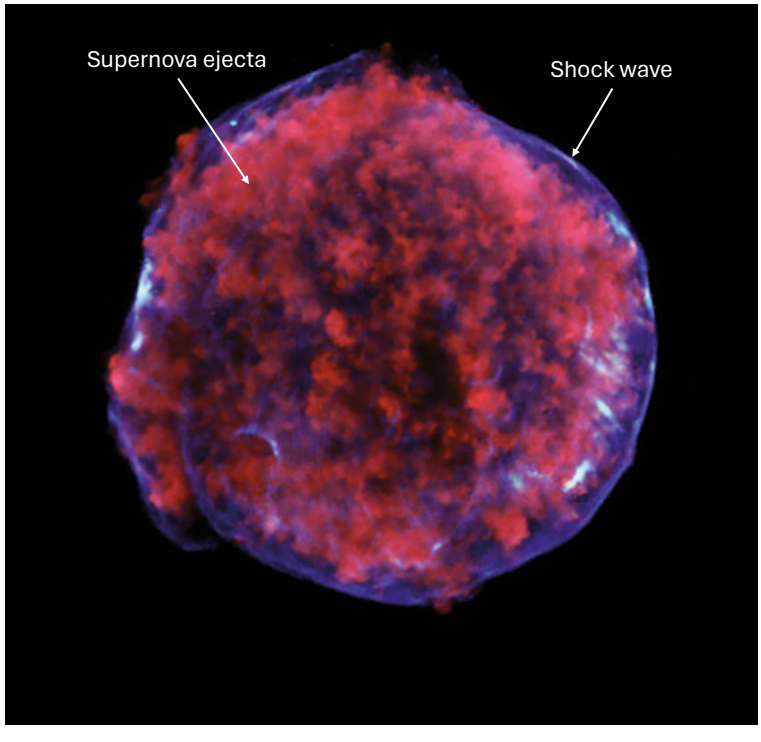

Figure 2.5. Image of the Tycho Supernova remnant taken by the Chandra X-Ray observatory. The red component is the low-energy X-ray emission from the ejecta of the SNR. The Blue component is the high-energy X-ray signature coming from the synchrotron emission of electrons being accelerated at the shock. Photo credit: NASA/CXC/Rutgers/K.Eriksen et al.

[5]The termination shock forms when the solar wind interacts with the surrounding interstellar medium.

Because of their inaccessibility to in situ measurements[6], the microphysics of astrophysical shocks remains an open question. The technology necessary to send any in-situ mission to even the closest SNR shocks is at least centuries away [7]. Until then, in-situ measurement of heliospheric shocks, complemented with computer simulations and remote sensing, are our greatest asset to explore the dynamics of collisionless shocks across the Universe.

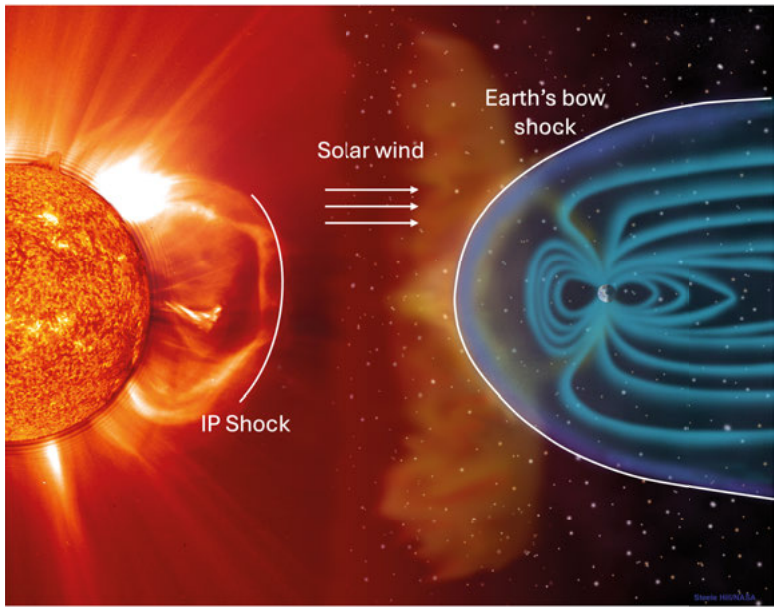

Figure 2.6. Artistic representation (not to scale) of an IP shock (left) ahead of a coronal mass ejection (CME) and Earth's bow shock (right) due to the interaction of the solar wind with Earth's magnetosphere. Photo credit ESA/NASA.

Observations of Earth's bow shock have been extremely valuable in driving our understanding of collisionless shock physics across the Universe, from exploring shock non-stationarity (Johlander et al., 2016; Madanian et al., 2021), to the various electrostatic and electromagnetic wave activity excited across the shock (Balikhin et al., 2005; Goodrich et al., 2018; Hull et al., 2012; Shi et al., 2023b; Wilson III, 2016), to particle acceleration (Johlander et al., 2021; Liu et al., 2019; Wilson III et al., 2016). Due to its proximity to Earth, it is the most studied shock using in-situ measurements, with many spacecraft crossing it regularly such as Cluster (Escoubet et al., 1997), THEMIS (Angelopoulos, 2009), and MMS (Burch et al., 2016) spacecraft to name a few. Earth's bow shock stands at $\sim 12-15\ R_E$ from the surface of Earth with R_E being the radius of Earth. It is a curved hyperbolically shaped shock (see Figure 2.6),

[6] And the limitation in computational power when it comes to real-life shock simulations.
[7] Maybe, when we are able to generate an artificial wormhole, we'll be able to send a multi-spacecraft mission to cross the Tycho SNR shock!

with a radius at the flanks reaching $\sim 27\ R_E$ (Balogh and Treumann, 2013). It forms due to the interaction between the supersonic solar wind and Earth's magnetosphere. Its curvature, along with the variability in the solar wind conditions makes Earth's bow shock extremely dynamical and hence the perfect laboratory for exploring the physics of collisionless shocks for a broad range of shock parameters[8].

[8]More on the key parameters controlling the dynamics of shocks in Chapter 3.

3. Key parameters controlling shock dynamics

The dynamics of shocks in collisionless plasmas are much more complex than their collisional hydrodynamic counterpart. As a starter the existence of a magnetic field in a plasma breaks the isotropy of the system. In regular hydrodynamics, there is no 'preferred' direction, the system is isotropic. On the other hand, in magnetized plasmas, a charged particle can stream freely parallel to the magnetic field, while it is restricted to gyrating motion perpendicular to the field. This breaks the isotropy of the system, adding complexity to the dynamics.

Furthermore, in collisional hydrodynamics, energy is dissipated by inter-particle collisions. While, as mentioned in Chapter 2, other mechanisms need to be active to explain energy dissipation in collisionless plasmas. Wave-particle interactions can generate such dissipation, but other means can be active as well depending on certain macroscopic parameters of the system.

In this Chapter, I will introduce two of the main macroscopic shock parameters controlling the dynamics of collisionless shocks.

3.1 Mach numbers

One of the main parameters controlling shock dynamics is the Mach number, M. It is the ratio between the upstream flow speed parallel to the normal to the shock, V_{un}, and the characteristic speed at which information propagates in the medium c, $M = \frac{V_{un}}{c}$. In regular hydrodynamics, $c = c_s$ is the sound speed in the medium. As seen in Chapter 2, in magnetized plasmas, there are three different speeds at which information can propagate: the fast-mode, the Alfvénic, and the slow-mode speeds. Therefore, three Mach numbers can be defined: the fast-mode $M_f = \frac{V_{un}}{c_f}$, the Alfvénic $M_A = \frac{V_{un}}{v_A}$, and the slow-mode $M_s = \frac{V_{un}}{c_s}$ Mach numbers.

For fast-mode shocks, the focus of study in this thesis, one characterizes its dynamics using both M_f and M_A. To form a fast-mode shock, M_f should be ≥ 1; by definition, M_A will also be > 1. One of the main physical processes controlled by the Mach number is the mechanism of energy dissipation across the shock. As noted in Chapter 2 the main mechanism invoked to explain the energy dissipation across collisionless shocks is anomalous dissipation due to wave-particle interactions. As the Mach number increases beyond a certain critical threshold, this anomalous dissipation will not have enough time to

dissipate the necessary energy to maintain the shock. This happens when the downstream plasma speed in the normal direction V_{dn} becomes less than the downstream sound speed c_s. In this case, downstream sound waves will be able to travel opposite to the direction of the flow, interact with the ramp, and steepen it even more causing it to have scales smaller than the anomalous dissipation scale (Kennel et al., 1985). This transition occurs at the first fast critical Mach number M_{fc}.

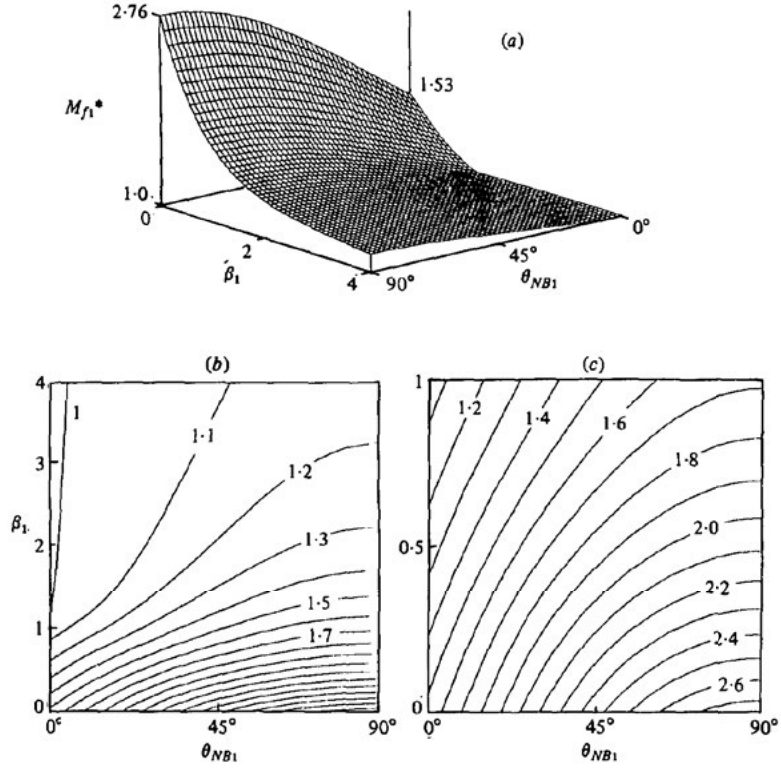

Figure 3.1. Parameteric dependence of the first critical Mach number for a heat capacity ratio $\gamma = 5/3$. Reprinted with permission from Edmiston and Kennel, 1984.

This critical Mach number was first predicted by Marshall, 1955, where they found a value of $M_{fc} \sim 2.7$ for a perpendicular shock. Beyond M_{fc}, to deal with the excess input of energy, the shock will start reflecting some of the incoming ions. When the ions reflect they will interact with the upstream flow causing it to become unstable and slowing it down before reaching the shock. The value of M_{fc} is highly dependent on other shock parameters such as the shock geometry quantified by θ_{Bn}[1], and β the plasma beta[2]. Figure 3.1 shows the dependence of M_{fc} on both θ_{Bn} and β from Edmiston and Kennel, 1984

[1]More on θ_{Bn} in the next section.

[2]The plasma beta is the ratio between the thermal and magnetic pressures in the plasma.

who did a parametric survey of the dependence of the critical Mach number on the various parameters of the shock. Shocks with $M_f \geq M_{fc}$ will be called throughout this thesis supercritical shocks.

A second critical Mach number exists, called the non-linear whistler critical Mach number M_{cnl}, defined with respect to the Alfvénic Mach number. If the Alfvénic Mach number of the shock increases beyond M_{cnl}, even ion reflection will not be enough to keep the shock stable and balance the non-linear steepening. The shock will therefore exhibit non-stationary behavior, either start breaking in on itself (Krasnoselskikh et al., 2002), or the shock surface will start rippling (Johlander et al., 2016).

The solar wind conditions at 1 AU make Earth's bow shock a fast-mode shock with fast-mode Mach number typically ranging between 4 and 7, and an Alfvénic Mach number running between 5 and 15 (Lalti et al., 2022a). For such high values of M_f Earth's bow shock is supercritical. Also, because of the relatively large variation in the solar wind conditions, in many instances, observations of non-stationary shocks have been made (Johlander et al., 2016; Madanian et al., 2021).

3.2 Shock geometry

As mentioned earlier, the dynamics of a charged particle parallel and perpendicular to a background magnetic field differ. Due to this anisotropy in dynamics, two types of collisionless shocks exist. The transition from one type to another is controlled by the geometry of the shock, quantified by θ_{Bn}, the angle between the vector normal to the surface of the shock $\hat{\mathbf{n}}$ and the upstream magnetic field $\mathbf{B}$.

Because of its curvature, Earth's bow shock is a great laboratory to explore the different dynamics of shocks with varying θ_{Bn}. Figure 3.2 shows a sketch of the bow shock around Earth taken and modified from Tsurutani and Rodriguez, 1981. The figure shows the interplanetary magnetic field (IMF) as the blue oblique lines, and the bow shock is highlighted with the white boundary. Two different types of shocks are evident. A well-defined and sharp shock transition in the bottom of the Figure where $\hat{\mathbf{n}}$ is almost perpendicular to the IMF, depicts the quasi-perpendicular portion of the shock, where $\theta_{Bn} > 45^\circ$. While a turbulent transition in the top of the Figure where $\hat{\mathbf{n}}$ is almost parallel to the IMF, i.e. $\theta_{Bn} < 45^\circ$, depicts the quasi-parallel shock transition.

For supercritical shocks, ions are reflected along the shock normal. If the shock is quasi-perpendicular, the reflected ions will have a large component of their upstream-directed velocity in the perpendicular direction to the upstream magnetic field. In response to this perpendicular field, they will gyrate back into the shock and gain energy from the upstream motional electric field[3]. This

[3]More on the details of ion dynamics at quasi-perpendicular shock, and its typical structure is given in Chapter 4.

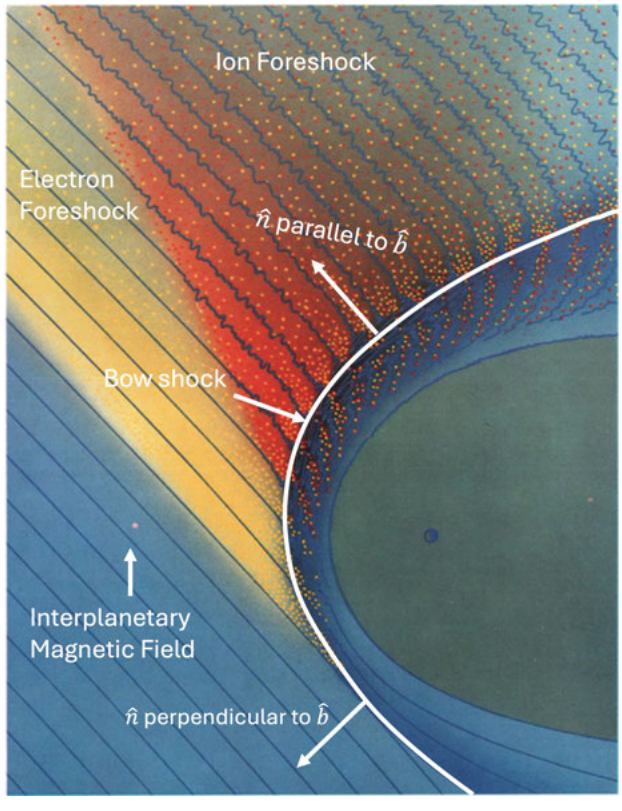

Figure 3.2. Schematics of the global dynamics of the bow shock around Earth formed from its interaction with the solar wind showing the distinction in dynamics between quasi-parallel and quasi-perpendicular shocks. Adapted from Tsurutani and Rodriguez, 1981.

reflected ion component will create a 'foot' ahead of the shock ramp, with a size comparable to the ion gyro-radius, where the solar wind is pre-decelerated and pre-compressed. A quasi-perpendicular shock crossing is a sharp transition from a stable and quiet upstream to a turbulent compressed downstream. Figure 3.3 panels (a-b) show the typical magnetic field and density signature of a quasi-perpendicular shock crossing with a clear sharp transition between upstream and downstream.

On the other hand, if the shock is quasi-parallel, the reflected ions will have a large velocity component parallel to the upstream magnetic field. In this case, the ions will be able to stream relatively freely into the upstream, interact with the incoming solar wind ions and electrons, and excite various types of instabilities before being convected back into the shock by the solar wind. This extended interaction region is called the foreshock upstream of the shock transition. It is a highly turbulent region, with many non-linear structures such as shocklets, SLAMS (Wilson III, 2016; Wilson III et al., 2009), foreshock

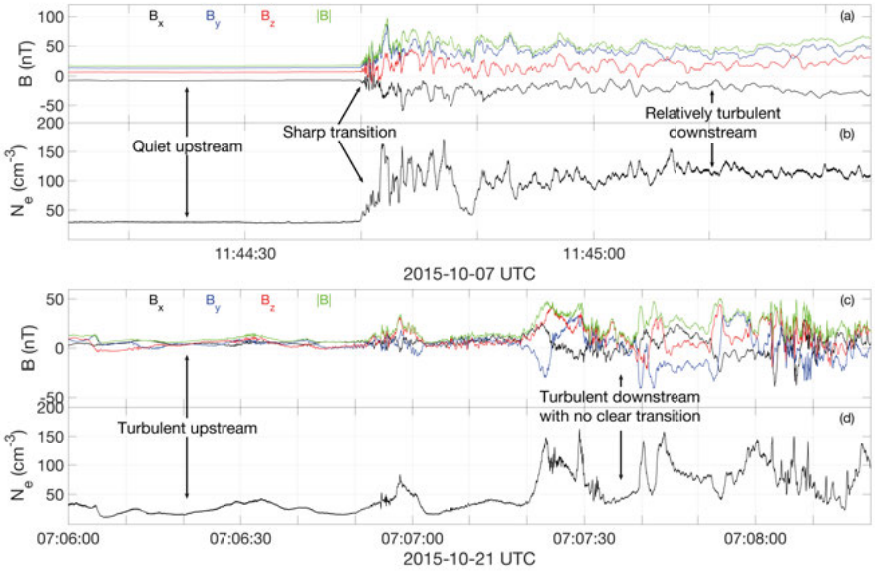

Figure 3.3. Two examples of Earth's bow shock crossings observed by the Magnetospheric Multiscale spacecraft (MMS). Panels (a-b) show the magnetic field and density for a quasi-perpendicular shock. Panels(c-d) show the magnetic field and density for a quasi-parallel shock.

bubbles, and hot flow anomalies (Turner et al., 2013). Some of those structures can themselves develop shocks in front of them and accelerate ions and electrons to relativistic energies (Johlander et al., 2021; Lalti et al., 2022a; Liu et al., 2019; Wilson III et al., 2016). For quasi-parallel shocks, unlike their quasi-perpendicular counterparts, it is difficult to identify the exact location of the shock transition. Figure 3.3 panels (c-d) show the typical magnetic field and density signature of a quasi-parallel shock crossing, with the clear disturbed and turbulent upstream, merging with the turbulent downstream, preventing a clear identification of a transition region.

Furthermore, at the point where the magnetic field is perpendicular to the shock normal the electrons and ions will experience a large mirroring force, and will reflect off of the shock, forming an energetic beam traveling parallel to the magnetic field and forming a boundary between the foreshock and the pristine solar wind called the foreshock boundary. Both species will eventually be convected back towards the shock due to the upstream solar wind motion. Since the electrons are much more mobile than the ions a separation occurs where an electron foreshock boundary and an electron foreshock forms without any reflected ions (the yellow-colored region in Figure 3.2). The electron foreshock will be followed by the ion foreshock boundary and the ion foreshock shaded in red in Figure 3.2.

The dynamics of quasi-parallel shocks are rich and interesting, but this thesis focuses on the dynamics and evolution of quasi-perpendicular shocks.

4. Particle dynamics at collisionless shocks

Quasi-perpendicular supercritical shocks are characterized by four different regions: the undisturbed upstream, the foot, the shock transition region characterized by a ramp, an overshoot and an undershoot, and the thermalized downstream. Each region has its distinct signature in the plasma parameters (i.e. magnetic and electric fields, plasma density, velocity, and temperature). A typical quasi-perpendicular supercritical shock crossing by the MMS spacecraft is shown in Figure 4.1[1]. The time series of the magnetic field magnitude, density, and bulk speed of the plasma are plotted in panels (a-c). While panels (d) and (e) show the phase space density reduced in the directions normal to the shock $\hat{n}$, and tangent to the shock but out of the coplanarity plane $\hat{t}_2$, respectively.

The spacecraft was initially in the pristine solar wind and moved[2] with time into the magnetosheath. The interval highlighted in blue shows the typical signature of the unperturbed solar wind with average parameters: $|B| \sim 9$ (nT), $N \sim 5\ \left(cm^{-3}\right)$, and $|V| \sim 400$ (km/s), well within the range of the typical solar wind parameters at 1 AU (Wilson III et al., 2021). The interval highlighted in cyan shows a slow increase in $|B|$ and N and a decrease in $|V|$, this is the typical signature of the shock foot formed by the reflected ions from the supercritical shock as described in Chapter 3.

The shock transition region is highlighted in red. The sharp increase in $|B|$ and N and the sharp decrease in $|V|$ signify the crossing of the shock ramp. A normal electric field exists within the ramp, pointing upstream in the direction normal to the shock surface. It is set up as a response to the different dynamics between the ions and electrons across the shock. The ramp scale size is determined by the dissipation mechanisms that balance the non-linear steepening of the shock and can range from ion down to electron scales depending on the macroscopic shock parameters (M_A and θ_{Bn}) (Bale et al., 2005; Krasnoselskikh et al., 2013, and references therein). The ramp is followed by an overshoot/undershoot region where the values of the magnetic field magnitude and density are enhanced and decreased above then below their downstream averages. This behavior is controlled by the currents set up by the various ion and electron populations in the ramp and downstream of the shock as will be detailed below. Finally, the spacecraft makes its way to the fully thermalized

[1]This is the same shock analyzed in Papers I. It has $M_A \sim 4.4$ and $\theta_{Bn} \sim 82^\circ$

[2]In reality, the speed of the spacecraft ($\sim 1-2$ km/s) is small compared to the speed of the shock ($\sim 10-100$ km/s). So it is the shock that convects upstream crossing the spacecraft.

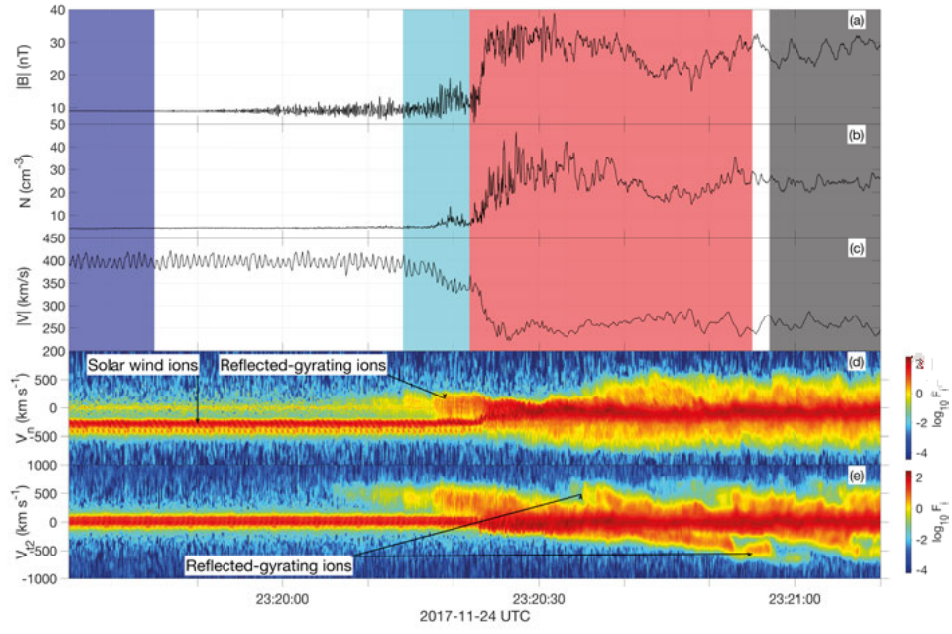

Figure 4.1. Typical signature of a quasi-perpendicular supercritical shock crossing observed by MMS. Panel (a) shows the magnetic field magnitude, panel (b) the ion density, panel (c) the ion speed, and panels (c) and (d) show the reduced ion distribution function along the shock normal and the direction out of coplanarity palen respectively. The upstream, foot, shock transition region, and downstream are highlighted in blue, cyan, red, and black respectively.

downstream, where the solar wind plasma has been decelerated, compressed, and heated (black-shaded interval).

In the solar wind, ion and electron dynamics are governed by the interplanetary magnetic field $\mathbf{B}$, and the convective electric field $\mathbf{E}_c = -\mathbf{V} \times \mathbf{B}$ in the shock rest frame. In such a crossed magnetic and electric field configuration, charged particle trajectories will combine two types of motion amounting to a trochoid[3]. The first is simple gyration around the magnetic field at the gyrofrequency $\omega_{cj} = \frac{q_j|\mathbf{B}|}{m_j}$, and the gyroradius $r_{cj} = \frac{v_{\perp j}}{\omega_{cj}}$, where q_j and m_j are the charge and mass of particle j, $|\mathbf{B}|$ is the magnetic field magnitude, and $v_{\perp j}$ is the particle velocity component perpendicular to the magnetic field. The second is a drift in the direction[4] perpendicular to both $\mathbf{E}_c$ and $\mathbf{B}$ equal to $\mathbf{v}_{E\times B} = \frac{\mathbf{E}_c \times \mathbf{B}}{B^2}$.

[3]A trochoid is the curve traced by a point fixed on a circle. Three types of trochoids exist, prolate, common, and curtate with the point fixed outside, on, and inside the circle respectively.
[4]This drift for the solar wind is generally radially outwards from the sun.

As both ions and electrons approach the shock, they start sensing gradients in the electric and magnetic fields, which will affect their dynamics. In turn, the dynamics of the charged particles will, self consistently, maintain the macroscopic and microscopic electric and magnetic fields across the shock. This interplay between the particles and the fields is what creates the distinct signatures of the foot, shock transition region, and downstream. This Chapter will highlight the dynamical response of both ions (section 4.1) and electrons (section 4.2) to the macroscopic and microscopic electric and magnetic fields across the shock, and the response of those fields to this particle dynamics.

4.1 Ion dynamics

When ions encounter the large gradients in **B** and **E** across the shock, they either decelerate and pass downstream, or reflect upstream. Figure 4.2 shows those two different types of trajectories obtained from a test particle simulation of a perpendicular shock. The upper panel shows the profiles of $|\mathbf{B}|$ and E_n, the normal electric field, across the shock, while the lower panel shows two different trajectories of an ion. The contours in the bottom panel are those of the magnetic field with blue(red) representing the value of $|\mathbf{B}|$ in the upstream(downstream). The trajectories are plotted in the plane perpendicular to $|\mathbf{B}|$, using the shock coordinate system with $\hat{n}$ being the shock normal pointing upstream, $\hat{b}$ is the unit vector pointing in the direction of $|\mathbf{B}|$, and $\hat{t}_2 = \hat{n} \times \hat{b}$ is out of the coplanarity plane and completes the right-handed system. In the solar wind $|\mathbf{V}_{\mathbf{E}\times\mathbf{B}}| >> v_{\perp i}$, hence the motion of ions will follow the shape of a curtate trochoid. The passing ions (dashed line) are decelerated by the normal electric field within the ramp, and convected downstream; they form the thermal ion population downstream of the shock[5]. On the other hand, the reflected ions (solid line) respond to both the magnetic and electric field gradients and reflect upstream. What differentiates the passing and reflected ions is their initial energy, pitch angle[6], and their phase at the time of encounter of the shock.

In their trajectory upstream of the shock, the reflected ions gyrate in the same direction as the convective electric field $\mathbf{E}_c$, gaining energy before coming back to the shock and crossing it. The signature of those two populations is evident in the reduced ion phase space density measured by MMS shown in panels (d) and (e) of Figure 4.1. The solar wind is the cold beam with peak phase space density at $(V_n,\ V_{t2}) \sim (-400,\ 0)$ km/s upstream of the shock. Within the foot, two ion components are evident, the solar wind beam traveling towards the shock, and the reflected-gyrating ion component with $V_n > 0$ and $V_{t2} > 0$ consistent with the trajectories shown in Figure 4.2.

[5]When the ions transition from upstream to downstream, their motion shifts from being a curtate trochoid to a prolate trochoid.

[6]The angle that the velocity vector makes with the background magnetic field.

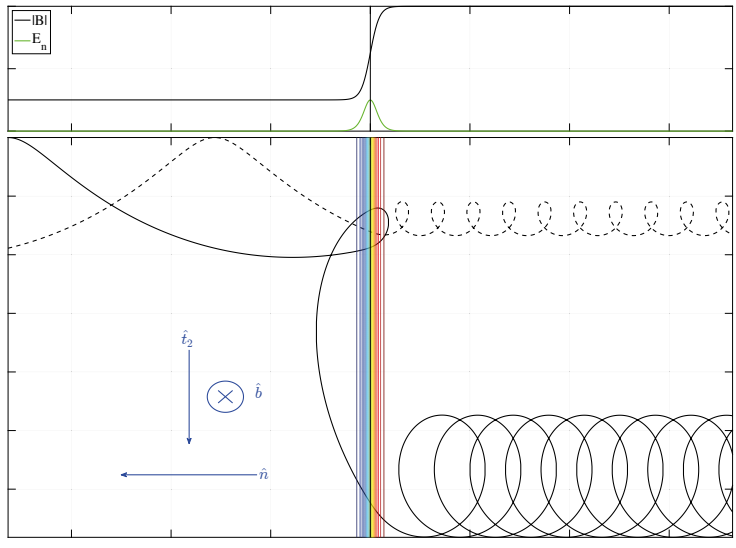

Figure 4.2. Typical trajectories of ions across quasi-perpendicular shocks from test particle simulation. The upper panel shows the profile of $|\mathbf{B}|$ and E_n used. The lower panel shows two trajectories one for a transmitted (dashed) ion and one for a reflected (solid) ion.

This reflected ion component modifies the plasma conditions locally in different ways. As a starter, a current will be set up in the foot in the $\hat{t}_2$ direction carried by the reflected ions. This current will cause the expected increase in the magnetic field magnitude and density in the foot. Also, the upstream flux of reflected ions will cause the bulk ion speed to decrease. To maintain a zero net current in the normal direction across the shock[7], the electrons will also be decelerated. So the solar wind plasma will be predecelerated within the foot.

The three drifting populations within the foot (incoming ions, incoming electrons, and reflected ions), constitute an unstable system where various plasma instabilities can be excited. The stability of such a system has been extensively studied in theory and simulations (Matsukiyo and Scholer, 2006; Muschietti and Lembège, 2017; Wu et al., 1984, and references therein). Three different drifts are sources of free energy for three different instabilities in the foot, the drift between the incoming and reflected ions, between the incoming electrons and reflected ions, and between the incoming ions and incoming electrons. Paper III looks at the waves in the foot from an observation point of view, where evidence is presented that whistler waves traveling upstream of the shock[8] are generated by the instability between the reflected ions and the incoming electrons.

[7] A condition for the stability of the shock.

[8] Those are the oscillation in the magnetic field shown in the upper panel of Figure 4.1.

Right downstream of the ramp, the reflected ions gyrate with a larger gyroradius compared to their transmitted counterpart, this is because they have been energized by the convective electric field as they gyrate in the foot. Due to the effect of the normal electric field, they are prevented from crossing the shock towards the upstream and continue their gyration downstream. Their phase space density signature is clear in Panel (e) of Figure 4.1, with oscillating V_{t2} (positive and negative) and energy larger than the core thermal population. Their gyration generates currents that drive the overshoot/undershoot structure beyond the ramp (Saxena et al., 2005). Furthermore, the ensuing ion distribution has a large perpendicular temperature anisotropy which in itself is a source of free energy that can drive various types of electromagnetic and electrostatic instabilities that work to isotropize the distribution and contribute to the irreversible energy dissipation across the shock (Wu et al., 1984).

4.2 Electron dynamics

The question of the response of the electrons to the large magnetic and electric field gradients of the shock is complex. So far, it has been observed that for supercritical shocks 10% of the inflow energy goes to electron heating and energization (Schwartz et al., 1988). Also, it is established that the downstream phase space density has the shape of a flat top (Feldman et al., 1983) (see Figure 4.3 for a typical flat top distribution observed by MMS downstream of a quasi-perpendicular shock). But how exactly is this 10% upstream inflow energy transformed to electron thermal energy, and what are the processes that shape the downstream flat top distribution remains an active field of research.

Two frameworks have been suggested to explain the electron dynamics across the shock. The first revolves around the adiabatic response of the electrons to the DC (large-scale) fields of the shock. The second revolves around the non-adiabatic response of the electrons to the AC (small-scale) oscillations in the fields across the shock.

4.2.1 The adiabatic framework

Within the adiabatic framework, because the shock ramp thickness is intermediate between electron and ion scales, one can assume that the electrons remain magnetized and the guiding center approximation is valid (Goodrich and Scudder, 1984; Lefebvre et al., 2007; Savoini and Lembege, 1994; Scudder, 1995). A suitable reference frame to analyze electron dynamics across the shock is the deHoffman Teller (HT) reference frame (De Hoffmann and Teller, 1950), where the inflow velocity is aligned with the upstream magnetic field and hence the convective electric field is zero.

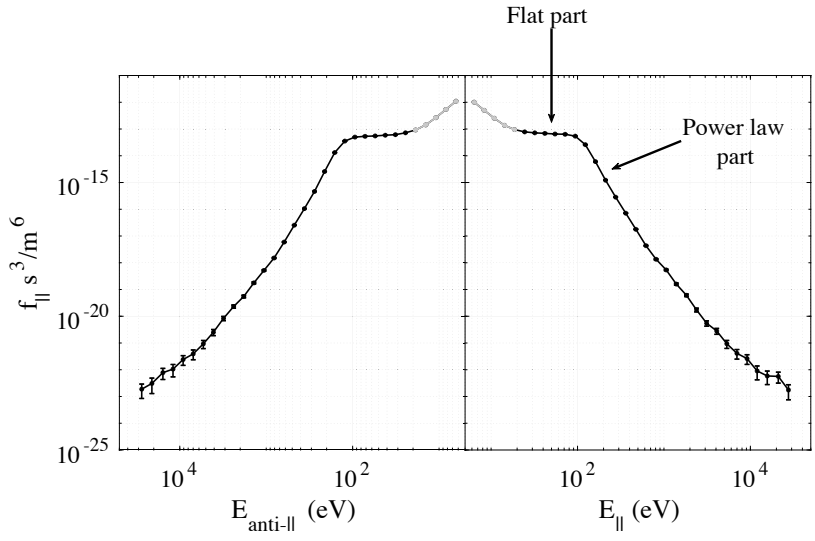

Figure 4.3. A parallel cut of the electron distribution function observed by MMS downstream of a quasi-perpendicular shock showing the typical signature of a flat top distribution. The low energy part of the distribution function highlighted in gray is an artifact of the instrument.

As a response to the increase in the magnetic field magnitude, and to conserve the first adiabatic invariant $\mu = \frac{m_e v_\perp^2}{|\mathbf{B}|}$, the electrons will increase their perpendicular energy as they cross the shock. On top of that, the normal electric field will accelerate the electrons in the direction parallel to the magnetic field. By assuming that the electrons conserve their energy one can write the equations for the downstream parallel ($v_{\|d}$) and perpendicular ($v_{\perp d}$) velocities of an electron as a function of their upstream values ($v_{\|u}$, and $v_{\perp u}$):

$$v_{\perp d} = \sqrt{\frac{|\mathbf{B}_d|}{|\mathbf{B}_u|}} v_{\perp u}, \tag{4.1}$$

$$v_{\|d} = \sqrt{v_{\|u}^2 + v_{\perp u}^2 \left(1 - \frac{|\mathbf{B}_d|}{|\mathbf{B}_u|}\right) + \frac{2e}{m_e}\Delta\Phi^{HT}}, \tag{4.2}$$

where $\Delta\Phi^{HT} = \Phi_d - \Phi_u$ is the cross-shock potential difference between the upstream and the downstream due to the normal electric field in the HT reference frame.

It is evident from Eq. 4.2 that for certain electrons with specific initial pitch angles and energies, the term under the square root is negative. Such electrons cannot overcome the mirroring force of the shock and are reflected upstream.

By taking advantage of Liouville's theorem, which states that the phase space density of electrons is conserved along electron trajectories $\frac{df}{dt}|_{traj} = 0$,

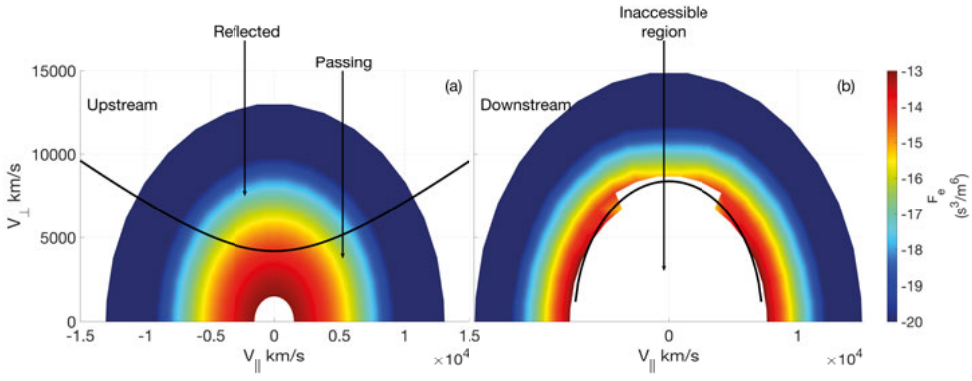

Figure 4.4. Modeled electron distribution functions in the $\left(v_{\parallel}, v_{\perp}\right)$ plane. Panel (a) shows a Maxwellian to model the solar wind distribution and panel (b) shows the resulting distribution after evolving the upstream Maxwellian in response to the DC fields of the shock using Liouville's theorem.

along with Equations 4.1 and 4.2, it is possible to model the evolution of a distribution in response to the DC fields of a shock. The results of such an exercise are shown in Figure 4.4, for $\frac{|\mathbf{B}_d|}{|\mathbf{B}_u|} = 4$ and $\Delta\Phi^{HT} = 150$ eV. Panel (a) shows a Maxwellian in the HT frame to model the solar wind distribution[9]. The x and y axis represent the velocity components parallel and perpendicular to the magnetic field. The black curve is the boundary between reflected and transmitted electrons, obtained by equating the term under the square root in Eq. 4.2 to zero. All electrons above this black line will reflect upstream, while the remaining electrons will be transmitted and form the downstream distribution shown in Panel (b). Two features in the downstream distribution are evident, the first is the inflation of the distribution reflecting the increase in the kinetic temperature of the electrons[10]. The second feature is the large void in the distribution at low energies, this region of phase space is inaccessible by the upstream electrons due to the effect of reflection.

[9]The observed solar wind distribution is more complex than that, having a core, halo, and Strahl components (Wilson III et al., 2019). For the sake of this analysis taking the core Maxwellian is sufficient.

[10]The second moment of the distribution divided by the zeroth moment.

At the boundary of this inner void (the black line) there exist large gradients in the distribution function, which are a source of free energy to various micro-instabilities. Such instabilities will smoothen the distribution at lower energies and form a flat top distribution. So, within the adiabatic framework, the main source of electron heating across the shock is the reversible adiabatic response to the macroscopic shock fields, while irreversible wave-particle interaction will smoothen and fill the resulting void, and cause a secondary non-adiabatic cooling.

Within the ramp, under the guiding center approximation electrons will drift in the $\hat{l}_2$ direction due to the $\mathbf{E} \times \mathbf{B}$ and ∇B drifts (Goodrich and Scudder, 1984; Krauss-Varban et al., 1989). Since the ions are demagnetized in the ramp, they will not follow this motion and a cross-field Hall current will set up in the ramp at the electron scales. The magnetic field generated by this current reinforces the overshoot (Krauss-Varban et al., 1989; Saxena et al., 2005). On top of that, the current acts as a free energy source for various instabilities within the ramp (Savoini and Lembege, 1994; Scudder et al., 1986).

4.2.2 The non-adiabatic framework

The most fundamental assumption of the adiabatic framework is that the electrons remain magnetized when crossing the shock. This assumption might not always be valid, and the electron adiabaticity can be broken in various ways across the shock. Figure 4.5 shows the same shock crossing shown in Figure 4.1, with panels (a) and (b) showing the magnetic and electric field time series and panels (c) and (d) their respective power spectral density obtained using a wavelet transform (Eriksson, 1998). One can see that in the foot, ramp, and downstream, there exists a large amplitude broadband spectrum of various electrostatic and electromagnetic waves. Each wave mode excited can resonate, scatter, and hence demagnetize the electrons.

As a starter, it has been shown that the existence of large electric field gradients can demagnetize and energize electrons locally, causing the inflation of the distribution function and the formation of a flat top (Balikhin et al., 1998; See et al., 2013). For high enough Mach numbers, the shock ramp width can be on electron scales (Krasnoselskikh et al., 2013). For those shocks, the variation of the DC fields across such small scales creates the necessary gradients to demagnetize the electrons. Furthermore, even for shocks with a ramp width on the order of ion scales, electric fields within the ramp can reach hundreds of mV/m as in the example of Figure 4.5 where panel (b) shows a ~ 600 mV/m peak-to-peak electrostatic structures. Panels (e) and (f) are zoom-ins on some of those high amplitude structures showing excitations of bipolar and monopolar structures which can be identified as phase space holes and double layers (Vasko et al., 2020; Vasko et al., 2018; Wang et al., 2020) and high amplitude ion acoustic waves (Balikhin et al., 2005; Goodrich et al., 2018; Vasko et al.,

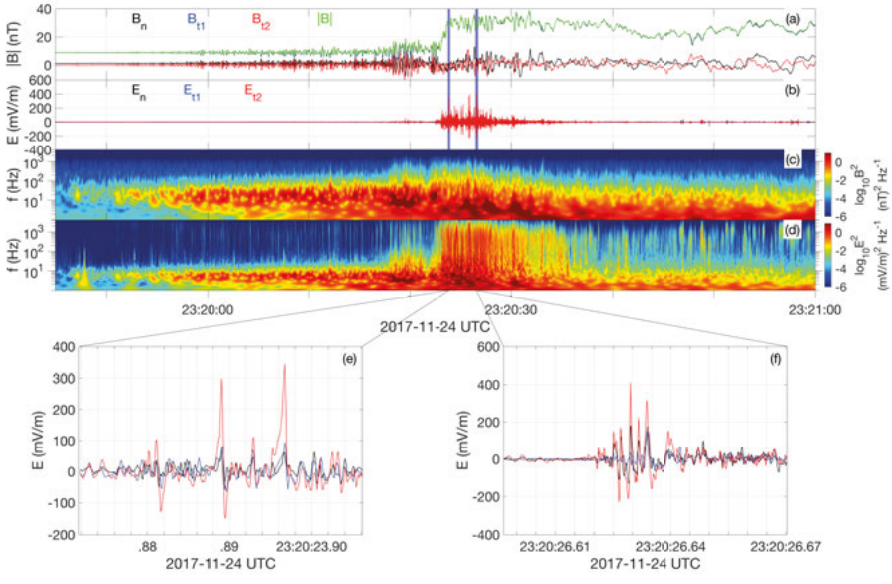

Figure 4.5. Typical quasi-perpendicular supercritical shock crossing by MMS highlighting the various wave activity across the shock. Panels (a) and (b) show the magnetic and electric field in the shock coordinate system (n, t_1, t_2). Panels (c) and (d) are the power spectral density of $|\mathbf{B}|$ and $|\mathbf{E}|$ respectively. Panels (e) and (f) are zoom-ins to some of the wave bursts observed in the ramp showing signatures for bipolar and monopolar structures and non-linear ion acoustic waves.

2022, and Chapter 7). Such oscillations are on the Debye scale and can scatter and demagnetize the electrons (Kamaletdinov et al., 2024; Kamaletdinov et al., 2022; Vasko et al., 2018) feeding the mechanism described by Balikhin et al., 1998 and See et al., 2013 forming a flat top.

Furthermore, high-frequency whistler mode waves (Amano et al., 2020; Shi et al., 2023a) and electrostatic ion-acoustic and solitary waves (Kamaletdinov et al., 2024; Kamaletdinov et al., 2022) can efficiently scatter the electrons and confine them within the ramp. While confined, the electrons gain energy from the convective electric field leading to an inflation of the downstream distribution and heating of the electrons (Amano and Hoshino, 2022; Kamaletdinov et al., 2024; Katou and Amano, 2019).

Even in the foot, large amplitude low-frequency whistler waves such as those seen upstream of the shock shown in Figure 4.5 can trap the electrons which in turn cause the growth of electron acoustic waves in a two-stage process leading to irreversible energy dissipation upstream of the ramp (Matsukiyo and Scholer, 2006; Muschietti and Lembège, 2017).

Paper V addresses the issue of electron heating across quasi-perpendicular shocks by analyzing the evolution of the electron distribution function across 310 MMS shock crossings.

5. The Magnetospheric MultiScale mission

The Magnetospheric Multiscale (MMS) mission (Burch et al., 2016), is a constellation of 4 spacecraft in a tetrahedral formation launched in 2015 with the primary objective of understanding electron scale physics in reconnection. It is equipped with multiple instruments that measure both fields and plasma parameters with high spatial and temporal resolution. Furthermore, the separation between the spacecraft reaches as low as ~ 5 km depending on the phase of the mission. This small separation along with the tetrahedral formation allows for the decoupling of temporal and spatial evolution of the plasma down to the electron scales. On top of that the tetrahedral formation allows the usage of methods such as the curlometer (Robert et al., 1998) or four spacecraft interferometry (Harvey, 1998) to determine various quantities needed to understand different plasma phenomena in space.

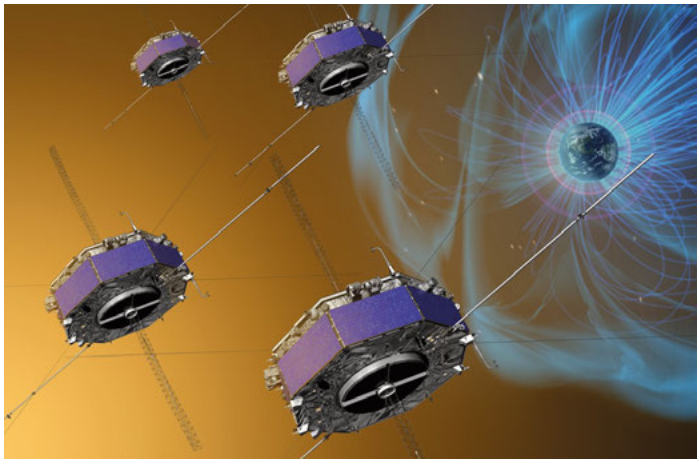

Figure 5.1. Artistic representation of MMS in orbit. Photo credit: NASA/GSFC.

Despite it being directed towards the physics of reconnection, MMS has proved to be valuable for the exploration of the physics of collisionless shocks. Multiple studies have been published in which data from MMS were analyzed to probe various open questions about collisionless shock physics from particle acceleration (Amano et al., 2020; Chen et al., 2018; Hanson et al., 2020; Johlander et al., 2023; Oka et al., 2017), to electrostatic and electromagnetic wave activity in and around the shock (Goodrich et al., 2018; Hull et al., 2020; Vasko et al., 2020), to shock reformation and rippling (Johlander et al., 2016;

Madanian et al., 2021; Yang et al., 2020), and even the observation of reconnection at quasi-parallel shocks (Gingell et al., 2019).

This chapter introduces the techniques employed by MMS to measure the main plasma and fields quantities used in this thesis. Namely, section 5.1 introduces the measurement of the ion and electron distribution functions along with their fluid moments. Sections 5.2 and 5.3 introduce the measurement of the electric and magnetic fields. Finally, section 5.4 introduces the multi- and single-spacecraft interferometry technique, used in Papers III, and IV respectively.

5.1 Particle distributions and moments

One of the successful techniques to measure particle distribution in space plasmas is the top-hat electrostatic analyzer (ESA). This technique has been implemented on various previous spacecraft such as on THEMIS (McFadden et al., 2008) or Cluster (Johnstone et al., 1997). Aboard MMS, the fast plasma investigation (FPI) instrument suite uses the same technology for both electron and ion measurements. Older spacecraft relied on the spin of the spacecraft to capture a full 3D distribution, which restricted the temporal resolution of the measured distributions to the spin period. To meet the science requirement for the time resolution, a novel implementation was designed in a way to break the spin rate limit and obtain 3D ion and electron distribution functions with the highest temporal and spatial resolution so far (Pollock et al., 2016).

A schematic of the FPI instrument design is shown in Figure 5.2. Panel (a) shows a bottom view of the spacecraft where 4 dual ion/electron spectrometers (DIS/DES) are distributed on the perimeter of the spacecraft. The dual spectrometer is formed by two top-hat ESAs at an angle from each. Each spacecraft has a total of 16 ESAs, 8 for ions and 8 for electrons. In this configuration, the measured distribution would have a 45° azimuthal resolution, which is not enough to meet the science requirement of the mission. Using electrostatic deflection of the field of view (FOV) increases the azimuthal resolution of the measured distribution to 11.25°.

Furthermore, each top-hat ESA has a 180° FOV in the polar direction divided into 16 sectors, giving a polar resolution of 11.25° as shown schematically in panel (b) of Figure 5.2. Finally, each electrostatic analyzer can resolve particles with energies from 10 eV to 30 keV logarithmically spaced, with $\Delta E/E = 14\%$. This provides a measurement of the 3D distribution function, discretized on a spherical logarithmic grid with $32\times16\times32$ resolution in Energy$\times$polar$\times$aximuth space. This design results in an unprecedented temporal resolution of 30 ms for the electrons and 150 ms for the ions.

The fluid moments (density, velocity, pressure tensor, and heat flux) can be obtained from the measured 3D distribution function by calculating the moments integral numerically on the spherical grid of the instrument.

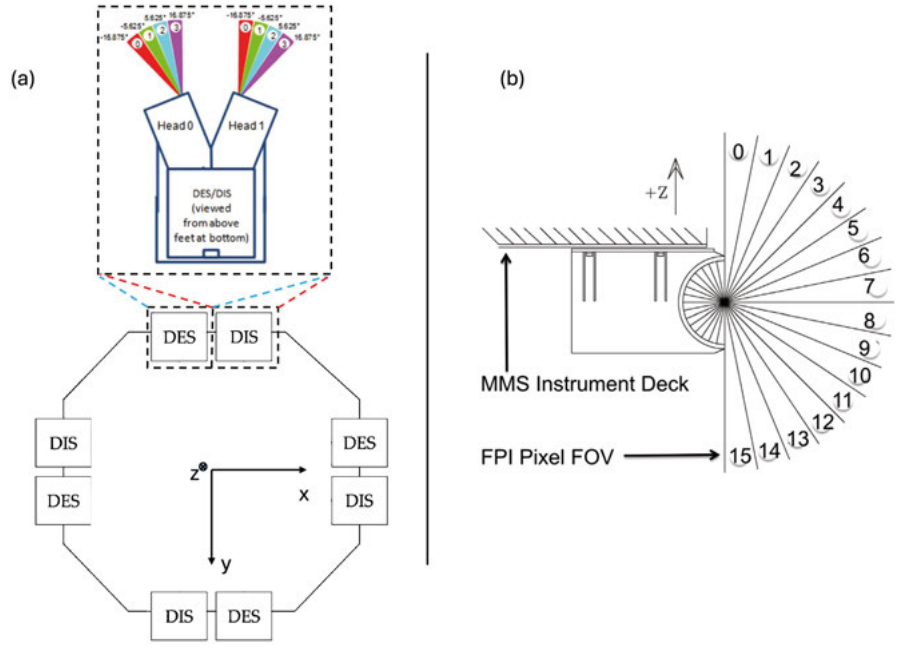

Figure 5.2. Schematics of the FPI instrument. Panel (a) shows a bottom view of the spacecraft with the distribution of the DES/DIS (bottom), and a zoom-in on the dual spectrometer configuration and the electrostatic deflection of the azimuthal field of view. Panel (b) shows a schematic of a single top-hat ESA from a side view, with the 180° FOV discretized at 11.25° resolution. Figure Adapted from Pollock et al., 2016.

When using the measurements of FPI one must note some instrument limitations that can affect the measured distributions and moments. For the measured distribution function, one must account for the effects of the spacecraft potential, photoelectron cloud, and secondary electrons on the measured distribution functions (Gershman et al., 2017). On top of that, especially at high energies, the density of particles hitting the detectors will be low, which will result in a high uncertainty on the value of the measured distribution (Gershman et al., 2015). Furthermore, due to the discretization of the distribution function and the limited energy range of the instrument, the moments might be over/underestimated[1]. In the analysis presented in this thesis, especially Papers III and V, such effects have been accounted for when necessary.

5.2 Electric field

Many techniques have been used to measure the electric field in space plasmas (Mozer, 1973). One of the most widely used techniques for this purpose is the

[1]Depending on various factors, such as the species analyzed and the location of the spacecraft.

double probe technique (Fahleson, 1967; Pedersen et al., 1998). In it, the gradient of the scalar potential V is approximated using a central difference scheme to obtain an estimate for the electric field.

This technique is used on MMS where a total of 6 probes in the double probe configuration allows for the measurement of the 3D electric field from DC up to $\sim$ 131 Samples/s. A schematic of the probe configuration on MMS is shown in Figure 5.3. Four spherical probes are in the spin plane forming the spin-plane double probes (SDP) (Lindqvist et al., 2016). Each double probe is separated by a distance of 120 m. The remaining two probes have a cylindrical geometry and are parallel to the spin axis of the spacecraft forming the Axial double probe (ADP) (Ergun et al., 2016). The probe-to-probe separation of the axial probes is $\sim$ 30 m.

In the double probe technique, spherical or cylindrical probes are set up in opposition to each other, each measuring the potential difference between the probe and the spacecraft (Maynard, 1998; Mozer, 2016; Pedersen et al., 1998). Using the measured probe-to-spacecraft potentials, the electric field is estimated using:

$$E_{ij} = -\frac{V_j - V_i}{d_{ij}}, \tag{5.1}$$

where E_{ij} is the electric field component pointing from probe i to probe j, $V_{i,j}$ is the probe to spacecraft potential for the probes i, j, and $d_{i,j}$ is the distance between probe i and j.

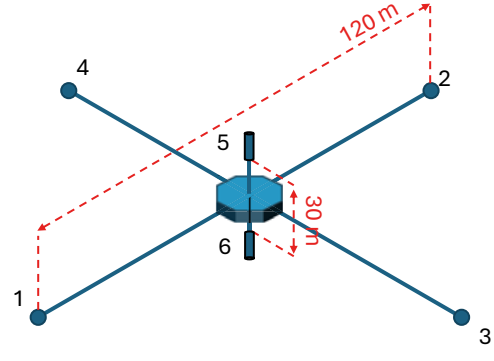

Figure 5.3. Schematic of the probe configuration on MMS.

As for any measurement method in science, the double probe technique has its limitations. One of those limitations is the short wavelength effects (Gurnett, 1998; LaBelle and Kintner, 1989; Lalti et al., 2023). The double probe technique works very well when d_{ij} is much smaller than the scale size of the electric field disturbance[2] L_s. When L_s becomes comparable to d_{ij}, the

[2]In the same way that the central difference approximation of a derivative works well the discretization length tends to zero.

measured electric field will be attenuated and phase shifted (Lalti et al., 2023). Other limitations to account for as well are the sheath impedance (Gurnett, 1998; Hartley et al., 2016) and the boom shorting (Califf and Cully, 2016; Pedersen et al., 1998) effects. In the analysis of Paper IV and the ongoing work in Chapter 7, the response of MMS to those effects has been analyzed and accounted for to properly characterize electrostatic waves across quasi-perpendicular shocks.

5.3 Magnetic field

Two Flux Gate Magnetometers (FGM) exist on MMS one Analog (AFG) and one Digital (DFG) (Russell et al., 2016) mounted on a 5-meter deployable boom. The FGM allows for the magnetic field measurement from DC up to 128 Samples/s, with a resolution of 0.1 nT and a range of $\pm$8000 nT.

Furthermore, to capture higher frequency magnetic field oscillations a search coil magnetometer (SCM) has been implemented on MMS (Le Contel et al., 2016). It is mounted on the same boom as that of the AFG and allows for the measurement of the magnetic field from 1 up to 16000 Samples/s.

The combination of the measurement of FGM and SCM allows for the detection of disturbances in the magnetic field from the shock ramp itself, to various electromagnetic wave modes excited by the shock with frequencies reaching the electron cyclotron frequency and above.

5.4 Multi and single spacecraft interferometry

Waves play an integral role in energy dissipation across collisionless shocks, but the characterization of the various wave modes excited remains an open question. Single spacecraft techniques (Sonnerup and Scheible, 1998; Wilson III et al., 2013) can be used to investigate this question. However, because a single spacecraft cannot decouple spatial and temporal variations, certain assumptions have to be made to extract the wave properties from the measured signal. Those assumptions might not necessarily hold. One of the most powerful methods to properly characterize a plasma wave[3], and decouple its spatial and temporal evolution is interferometry (Balikhin et al., 1997a; Graham et al., 2016; Lalti et al., 2023, 2022b; Steinvall et al., 2022).

Assume a simple plane wave disturbance of the form $f = \delta f \exp i(\mathbf{k}\cdot\mathbf{r} - \omega t)$, where f represent any measurable plasma quantity such as magnetic field, electric field, density, etc... δf is its amplitude, $\mathbf{k}$ is the wave normal vector, $\mathbf{r}$ is the displacement vector, and ω is the angular frequency. Interferometry re-

[3] linear or non-linear

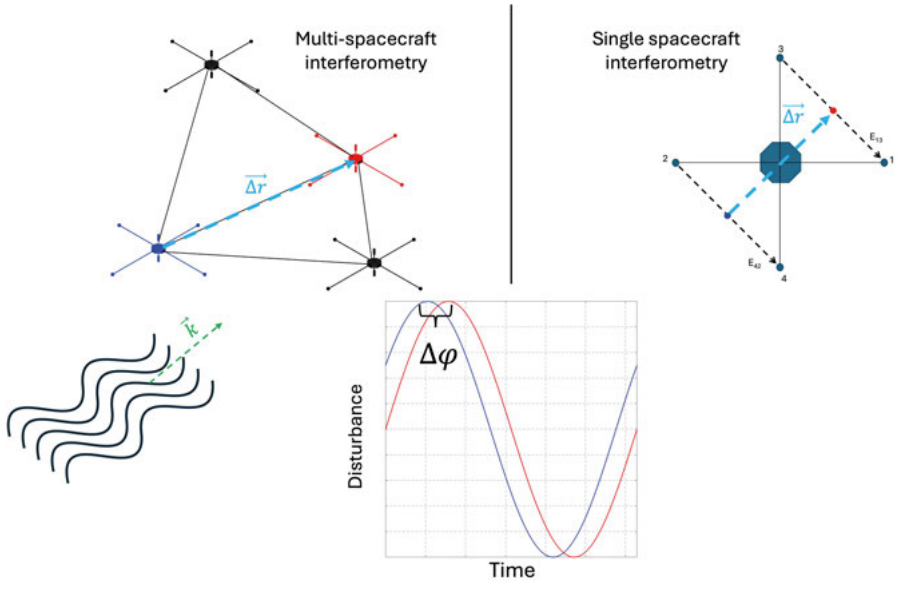

Figure 5.4. Schematic explaining multi and single spacecraft interferometry. The top shows MMS in its tetrahedral formation (left) and a top view of a single MMS spacecraft (right). The bottom blue and red curves are the signature of the disturbance (left corner) in the data as it passes the two measurement points color-coded in blue and red.

quires the simultaneous[4] measurement of f at two[5] different locations in space $\mathbf{r}_1$ and $\mathbf{r}_2$. The two measurements will have a phase shift of $\Delta\phi$, which obeys the relation

$$\Delta\phi = \mathbf{k} \cdot \Delta\mathbf{r}, \tag{5.2}$$

where $\Delta\mathbf{r} = \mathbf{r}_2 - \mathbf{r}_1$ is the separation vector between the two measurement points (see Figure 5.4). Knowing $\Delta\mathbf{r}$, one can determine the component of the wave vector along its direction $\mathbf{k} \cdot \frac{\Delta\mathbf{r}}{|\Delta\mathbf{r}|}$.

For the interferometry technique to work, $|\Delta\mathbf{r}|$ has to be smaller than half of the wavelength of the wave of interest, otherwise the signal will be spatially aliased. On top of that $|\Delta\mathbf{r}|$ has to be large enough to measure a phase shift between the two signals. Using MMS one can apply multi or single spacecraft interferometry to explore the characteristics of waves across scales. The typical separation between the 4 MMS spacecraft is of the order of 10^1 km. Paper III uses multi-spacecraft interferometry, for the first time, to properly characterize electromagnetic whistler waves with a wavelength of the order of the ion inertial length $\sim 10^2$ km, that play a major role in the dynamics of

[4]This can be generalized to include measurements with time delays as well (Balikhin et al., 1997a).
[5]Or multiple.

collisionless shocks. Furthermore, the probe-to-probe separation of the spin plane electric field probes on MMS is 120 m. Paper IV uses single spacecraft interferometry to properly characterize electrostatic waves with wavelength comparable to the Debey length $\sim 10^2$ m, which are believed to play an integral role in the energy dissipation across the shock. A visual summary of the multi and single-spacecraft interferometry techniques is shown in Figure 5.4.

6. Summary of papers

6.1 Paper I

Automated Classification of Plasma Regions Using 3D Particle Energy Distributions
Olshevsky, V., Khotyaintsev, Y. V., **Lalti, A.**, Divin, A., Delzanno, G. L., Anderzén, S., Herman, P., Chien, S. W. D., Levon, A., Dimmock, A. P., Markidis, S.
Journal of Geophysical Research (Space Physics), vol. 126, no. 10, 2021.
doi:10.1029/2021JA029620.

The Magnetospheric MultiScale (MMS) mission is a constellation of 4 spacecraft launched in 2015, equipped with high-resolution instruments providing in-situ measurements of both fields and plasma quantities. In its orbit, MMS crosses different plasma environments, from the pristine solar wind (SW) to the ion foreshock (IF), to the magnetosheath (MSH) to the magnetosphere (MSPH). Each of those regions is identified with its characteristic signature in the data. To investigate the various physical phenomena of each of those regions scientists have to go through terabytes of data sent by MMS to look for the signatures of interest, which is laborious work. In this study we train a convolutional neural network (CNN) to automatically identify the signature of 4 different regions, SW, IF, MSH, and MSPH, using the skymap ion distribution functions measured by the Dual Ion Spectrometers (DIS) aboard MMS. The CNN returns the probability that MMS is in one of the four regions of interest. By comparing the output of the CNN to the human labels of the different regions we find that the CNN can correctly identify the region that MMS is in with 98% accuracy.

My contributions:
I provided the training set used to train the CNN and contributed to the writing, reviewing, and proofing of the manuscript.

6.2 Paper II

A Database of MMS Bow Shock Crossings Compiled Using Machine Learning
Lalti, A., Khotyaintsev, Y. V., Dimmock, A. P., Johlander, A., Graham, D. B., and Olshevsky, V.
Journal of Geophysical Research (Space Physics), vol. 127, no. 8, 2022.

doi:10.1029/2022JA030454.

The high-resolution particle and field measurements by MMS provide an unprecedented opportunity to explore the kinetic physics of Earth's bow shock. In this study, we use the probability outputs from the CNN developed in Paper I to compile a database of MMS shock crossings. We do so by looking for intervals when MMS crosses from the solar wind or the ion foreshock to the magnetosheath and vice versa, which we identify as shock crossings. The database is the largest to date, containing 2797 shocks. For each of those shocks, we provide key shock parameters such as the shock normal, Alfvénic and fast-mode Mach numbers, the angle between the shock normal and the upstream magnetic field θ_{Bn}, plasma beta, the magnetic and density compression ratios to name a few. The database covers a broad and unbiased range in parameter space.

We also provide key spacecraft parameters, such as spacecraft separation and location at the time of the crossing. Furthermore, for each shock, we provide an overview plot containing key quantities such as magnetic and electric fields, density, velocity, ion and electron distribution functions along with other quantities. We expect that this database will be a great asset to the shocks community.

We also demonstrate the usefulness of the database by performing a statistical study of ion acceleration efficiency at the bow shock. We show that quasi-parallel shocks are more efficient at accelerating ions than their quasi-perpendicular counterparts in agreement with previous works.

My contributions:
I compiled the database, performed the data analysis, and had the main responsibility of writing the paper.

6.3 Paper III

Whistler Waves in the Foot of Quasi-Perpendicular Supercritical Shocks
Lalti, A., Khotyaintsev, Y. V., Graham, D. B., Vaivads, A., Steinvall, K., and Russell, C. T. Journal of Geophysical Research (Space Physics), vol. 127, no. 5, 2022.
doi:10.1029/2021JA029969.

Whistler waves play a major role in the dynamics of quasi-perpendicular collisionless shocks. They have been observed using spacecraft measurement upstream of the quasi-perpendicular part of Earth's bow shock since the 70s, their characterization relied on single spacecraft techniques, while their generation mechanism is still under debate. In Paper III, for the first time, we use multi-spacecraft interferometry to characterize whistler waves upstream of 11 quasi-perpendicular supercritical shocks observed by MMS. We find that the

waves propagate obliquely to the background magnetic field with an angle ranging from 20° to 42°. They also propagate obliquely to the shock normal and mainly within the coplanarity plane. In the plasma rest frame, the waves have a frequency comparable to the lower hybrid frequency (f_{LH}) in the range $[0.3\ 1.2]f_{LH}$, and a wavelength in the range [0.7 1.7] ion inertial lengths.

Many theories have been proposed to explain the generation of those waves, from micro-instabilities in the foot and the ramp of the shock, to shock non-stationarity, to shock dispersion. We use the high-resolution ion and electron distribution functions measured by MMS, along with a linear dispersion solver, to show that the most likely source of the waves is the kinetic cross-field streaming instability between the reflected ion beam and the incoming solar wind electrons.

My contributions:
I performed the data analysis and had the main responsibility of writing the paper.

6.4 Paper IV

Short-Wavelength Electrostatic Wave Measurement Using MMS Spacecraft
Lalti, A., Khotyaintsev, Y. V., and Graham, D. B. Journal of Geophysical Research (Space Physics), vol. 128, no. 4, 2023.
doi:10.1029/2022JA031150.

Short-wavelength electrostatic waves are believed to play a key role in energy dissipation in collisionless space plasmas. Their study requires reliable measurement of the wave electric field. In Paper IV we show that the double probe technique, employed by MMS to measure the electric field, fails at giving reliable measurements for short wavelength waves, due to the wavelength of the waves being comparable to the probe-to-probe separation. At such small wavelengths, the measured electric fields are systematically biased towards the axial direction, preventing reliable determination of the modes of the observed waves.

We develop a method, based on single spacecraft spin-plane interferometry coupled with modeling of the response of the spacecraft to a short-wavelength wave, to measure the 3D dispersion relation of short-wavelength electrostatic waves. The method assumes that we are measuring plane waves, with wavelengths larger than 45m and propagation direction not aligned with the axial probes resulting in a measurable spin-plane electric field. We test the method initially on synthetic data, then on waves whose properties are generally known, namely ion-acoustic waves in the solar wind. Previous studies of the properties of ion-acoustic waves in the solar wind showed that they propagate predominantly parallel to the background magnetic field. We con-

firm this expectation using our method, and we show that the waves have a wavelength of the order of 10^1 Debye lengths.

My contributions:
I developed the method, performed the data analysis, and had the main responsibility of writing the paper.

6.5 Paper V

Electron heating at quasi-perpendicular collisionless shocks
Lalti, A., Khotyaintsev, Y. V., and Graham, D. B.
Manuscript Submitted.

One of the remaining open questions in collisionless shock physics is that of electron heating and energization across the shock. Two competing frameworks have been suggested to address this question, revolving around the adiabatic and the non-adiabatic electron dynamics across the shock respectively. In Paper V, we use the database developed in Paper II along with the high-cadence in-situ measurements by the Magnetospheric MultiScale (MMS) spacecraft to study electron heating across 310 quasi-perpendicular shocks. By using a Liouville mapping technique, and by calculating the spectral index of the suprathermal electrons, we find, for the first time, that no single mechanism controls electron heating across the shock. We find that the heating mechanism is controlled by a macroscopic shock parameter, namely, the Alfvénic Mach number in the deHoffman Teller frame. We also find that for high Mach number shocks, the electron dynamics are consistent with the predictions of the Stochastic Shock Drift Acceleration (SSDA) mechanism.

My contributions:
I performed the data analysis and had the main responsibility of writing the paper.

7. Outlook

Our understanding of the physics of collisionless shocks has come a long way since the field's inception in the fifties. However, many unanswered questions remain to be explored, spanning the scales from the global dynamics of the bow shock and its response to the solar wind turbulence, down to the electron and Debye scales where the main irreversibility is expected to occur. In this Chapter, I will discuss some ongoing works and possible future projects relevant to the exploration of the physics of collisionless shocks.

Starting from the smallest scales, as has been discussed in Chapter 4, Debye scale electrostatic waves play an integral role in the dynamics of collisionless shocks. Using the interferometry-based method developed in Paper IV, we are exploring the evolution of such waves across quasi-perpendicular shocks. We have analyzed the electrostatic wave activity across the MMS shock crossing shown in Figure 4.5. We calculate the main wave properties, such as frequency and phase speed in the plasma rest frame, the wavelength, and the angle between the wave vector and the background magnetic field, θ_{kB}, for over 600 electrostatic wave bursts spanning the whole MMS shock crossing shown in Figure 4.5, from the upstream to the downstream.

The preliminary results of this analysis are shown in Figure 7.1. In panel (a) we show the magnetic field time series and highlight three different regions. The upstream and foot region is highlighted in blue, the shock transition region in black, and the downstream in red. Panels (b-e) shows the histograms of $\sin\theta_{kB}$, the wavelength λ, the wave frequency in the plasma rest frame f_{pl} normalized to the ion plasma frequency f_{pi} and phase speed V_{pl} normalized to the sound speed c_s respectively for the wave bursts analyzed in the three different regions. Two main results can be directly noted. In the upstream region (blue histograms), one can distinguish between two populations of waves one with $f_{pl}/f_{pi<1}$, $V_{pl}/c_s \sim 1$ and $\lambda \sim 250$ m and the other with $f_{pl}/f_{pi>1}$, $V_{pl}/c_s \sim 10^1$ and $\lambda \sim 350$ m with both being predominantly field-aligned and both having an acoustic-like dispersion relation. The higher frequency component is highly dispersive with frequency reaching ~ 20 kHz and is modulated by the lower-hybrid frequency electromagnetic whistler waves in the upstream (not shown), possible wave modes consistent with this observation are electron acoustic waves (Berthomier et al., 2000; Matsukiyo and Scholer, 2006) or beam mode waves (Onsager and Holzworth, 1990).

Furthermore, in the upstream and downstream, θ_{kB} for all the waves is predominantly field-aligned (see blue and red histograms in panel b). It shifts to predominantly perpendicular within the shock transition region (black histogram in panel b).

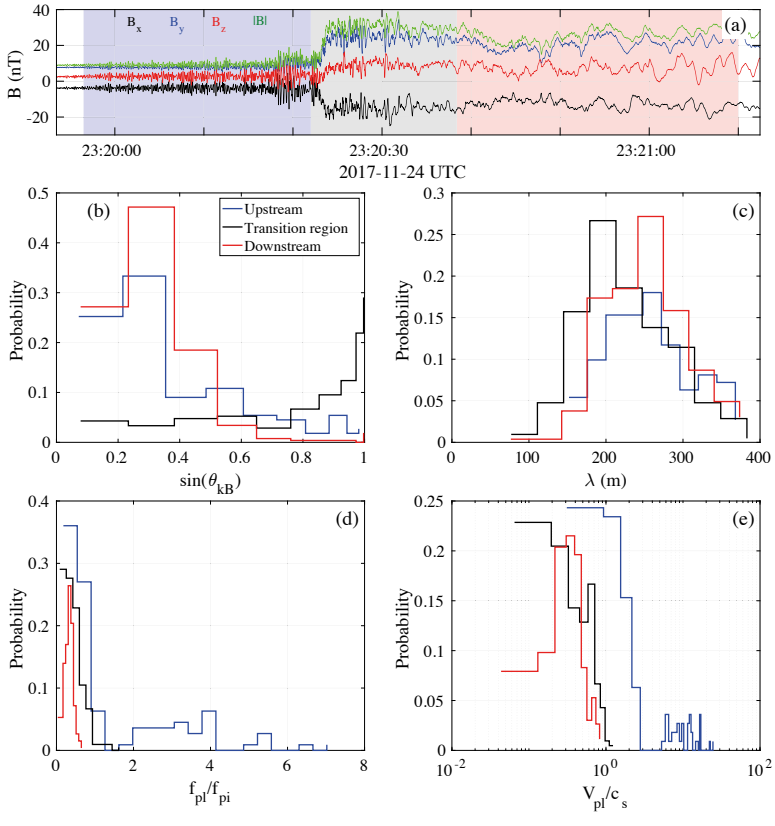

Figure 7.1. Prelimenary result of the ongoing investigation of Debye-scale electrostatic waves across the shock. Panel (a) shows the magnetic field time series with the upstream, shock transition region and downstream shaded in blue, black, and red respectively. Panels (b-e) shows the probability distribution of $\sim \theta_{kB}$, λ, f_{pl}/f_{pi}, and V_{pl}/c_s respectively. The blue, black, and red histograms correspond to the upstream, shock transition region, and downstream respectively.

Work is ongoing to identify the various wave modes observed along with their generation mechanism for this shock. In addition, such statistical results are essential for understanding the effect of the interaction between the electrons and Debye scale electrostatic waves (Kamaletdinov et al., 2024), yet the results we have so far are not generalizable, as they come from a single shock crossing. We are currently in the process of applying the same analysis at multiple shock crossings with varying M_A, θ_{Bn}, and plasma beta.

When it comes to the question of small-scale electrostatic waves, MMS has limited capabilities. The method of Paper IV is limited to resolving waves with wavelengths in the range [45, 500] m, while the excited waves might be anywhere outside of that interval. On top of that, as mentioned earlier, the electric field of such small wavelength waves is affected by different instrumental effects. Future missions, such as ESA's Plasma Observatory, and

NASA's MAKOS, are equipped with electric field instruments that mitigate the problems faced with MMS and allow for the accurate exploration of the Debye scale physics at Earth's bow shock.

As for the question of electron heating, Paper V analyzed the kinetic behavior of electrons across the shock. However, the dynamics of electrons can be described using a two-fluid description and closing the system with either an equation of state or the CGL closures (Baumjohann and Treumann, 2012). Work is currently ongoing to compare the validity of the different frameworks using the shocks list of Paper V. In particular, we find a value of the adiabatic index $\gamma \sim 1.43$ lower than previous empirical estimates of around ~ 2.4 (Hull et al., 2000; Schwartz et al., 1988), and lower than the theoretical value of $5/3$ for a monatomic gas with 3 degrees of freedom (Leroy et al., 1982; Masters et al., 2011). In addition, the CGL closure holds under only certain restrictive assumptions that are not mostly expected to be satisfied at collisionless shocks (Chew et al., 1956; Schwartz, 2014; Scudder et al., 1986). Nevertheless using in-situ data, we find relative agreement between observations and the predictions of this closure, consistent with previous studies (Schwartz et al., 1988). As a preliminary result, we find that this agreement is dependent on the upstream electron plasma beta. Work is ongoing to explore this topic further.

Going up in scale, beyond a certain Mach number the shock starts to exhibit non-stationary behavior (Krasnoselskikh et al., 2002; Krasnoselskikh et al., 2013; Lowe and Burgess, 2003). This is a regime of dynamics that is still poorly explored; multipoint measurements have been used to observe and study the shock dynamics in this regime (Johlander et al., 2016; Madanian et al., 2021; Yang et al., 2020), but many open questions remain. For example, our understanding of particle dynamics across the shock assumes a stationary structure, while time-dependent behavior can modify the shock properties locally affecting the plasma turbulence within the shock and opening up new pathways for particle energization and acceleration.

The focus has been so far on quasi-perpendicular shocks, but their quasi-parallel counterpart is richer in dynamics. One of the open questions to tackle is that of particle acceleration. Quasi-parallel shocks are more efficient than quasi-perpendicular ones at accelerating ions (Johlander et al., 2021; Lalti et al., 2022a). While for electrons, the plasma turbulence in the foreshock provides an efficient confinement for them to be accelerated and reach relativistic energies (Liu et al., 2019; Wilson III et al., 2016). The high-resolution data by MMS provides a great opportunity to explore the dynamics of hot flow anomalies and foreshock bubbles (Turner et al., 2013) and their role in particle energization at quasi-parallel shocks.

Observations of Earth's bow shock give us access to a limited range in shock parameter space, specifically, the Mach number values typically range within $[5, 15]$. Such restrictions can be overcome by analyzing in-situ measurement of shock crossings elsewhere in the heliosphere, such as IP shocks with ESA's

Solar Orbiter, and NASA's Parker Solar Probe, or at Jupiter using JUICE, at Saturn using Cassini, at Mars using Maven, and at Venus using Venus Express. This will expand greatly the range of parameter space explored.

Finally, despite being a great asset in pushing our knowledge about collisionless shocks, in situ observations, using the current space missions in operation, have their limitations. Great benefits can result from supplementing in-situ observations with results from large and small-scale numerical simulations.

8. Sammanfattning på svenska

En chockvåg i luft är en tunn diskontinuitet som uppstår när ett föremål, till exempel en kula eller ett stridsflygplan, färdas med en hastighet som är större än ljudhastigheten. Över chocken bromsas flödet till hastigheter lägre än ljudhastigheten och luften upphettas. Uppvärmningen sker vanligen genom kollisioner mellan partiklar. I rymden är chockvågor mycket vanliga, de förekommer i supernovarester (SNR), aktiva galaxkärnor (AGN), gränsskiktet mellan heliosfären och det interstellära mediet eller gränsytan mellan solvinden med överljudshastighet och jordens magnetfält. Men i rymden är densiteten ofta så låg att kollisioner mellan partiklar saknar betydelse på chockens längdskala. Detta är kollisionsfria chocker och deras exakta dynamik är fortfarande en av de återstående öppna frågorna inom fysiken.

Det är allmänt accepterat att våg-partikel-växelverkan kan spela samma roll som kollisioner och orsaka irreversibel dissipation av energi över kollisionsfria chocker. Men exakt hur detta går till undersöks fortfarande. I denna avhandling fokuserar vi på att studera de elektrostatiska och elektromagnetiska vågor som genereras och hur dessa påverkar upphettning av elektroner över jordens kvasi-vinkelräta bogchock (där solvinden bromsas upp) med hjälp av direkta mätningar "in situ" med instrument ombord på NASA:s Magnetospheric MultiScale (MMS) satelliter. MMS består av fyra rymdfarkoster uppsända 2015 som kretsar runt jorden i tetraeder-formation. Satelliterna är utrustade med vetenskapliga instrument med hög rums- och tidsupplösning för att mäta fält och partiklar som gör det möjligt att studera fysik på elektronskalor vid jordens bogchock.

I sin omloppsbana korsar MMS olika plasmamiljöer, var och en med karakteristiska signaturer i data. I artikel I tränar vi ett neuralt nätverk (convolutional neural network, CNN) att automatiskt identifiera olika områden som MMS passerar. CNN-nätverket är tränat på fördelningsfunktioner av joner observerade av MMS och returnerar sannolikheten att rymdfarkosterna befinner sig i en av fyra regioner: den ostörda solvinden, jonförchocken, magnetoskiktet och magnetosfären.

För att hitta intervall när MMS korsar bogchocken skulle man behöva gå igenom terabyte av data som skickats av MMS vilket vore ett mödosamt arbete. I artikel II använder vi sannolikheterna från CNN-nätverket utvecklat i artikel I för att automatiskt identifiera passager av bogchocken. Vi letar efter intervaller när MMS passerar från solvinden eller jonförchocken till magnetoskiktet, och vice versa, vilket vi identifierar som en passage av bogchocken. På detta sätt sammanställer vi en databas med 2797 chocker. För var och en

av dessa chocker ger vi viktiga parametrar som Alfvén- och andra Mach-tal, vinkeln mellan magnetfältet uppströms i solvinden och normalen till chocken θ_{Bn} och plasma β för att nämna några. Vi ger också översiktsfigurer som visar utvecklingen i tiden av flera fält- och plasmaparametrar. Vi tror att en sådan databas kommer att vara till stor hjälp för forskare som är intresserade av chocker.

Elektromagnetiska visslar-vågor tros spela en stor roll i utvecklingen av kollisionsfria chocker, eftersom de kopplar jonernas dynamik till elektronernas. Dessa vågor har studerats tidigare med observationer från enstaka rymdfarkoster, men hur de genereras diskuteras fortfarande. I artikel III använder vi för första gången observationer från fyra satelliter för att undersöka visslarvågor framför 11 passager av en kvasi-vinkelrät bogchock. Vi visar att sådana vågor har en våglängd av samma storleksordning som den så kallade tröghetslängden för joner och utbreder sig snett mot bakgrundsmagnetfältet. Genom att undersöka fördelningsfunktionerna av joner och elektroner observerade av MMS vid foten av chocken, och genom att numeriskt studera vågornas dispersionsrelation, visar vi att den mest rimliga mekanismen för att generera vågorna är en instabilitet mellan inkommande elektroner i solvinden och joner reflekterade av chocken.

I artikel IV ändrar vi fokus och studerar elektrostatiska fluktuationer på Debye-skala som exciteras över chocken. Dessa når icke-linjära amplituder med elektriska fält upp till 10^2 mV/m, bland de högsta uppmätta i jordens närhet. Man tror att dessa vågor spelar en viktig roll för dissipation av energi i kollisionsfria chocker. Ändå återstår många viktiga frågor vad gäller att karaktärisera vågorna samt hur vågorna genereras och deras växelverkan med både joner och elektroner. I artikel IV utvecklar vi en metod baserad på interferometri av elektriska fält observerade i spin-planet på en satellit för att studera dispersionsrelationen, inklusive 3D-riktningen av utbredning och våglängd, av elektrostatiska strukturer på Debye-skala observerade med MMS. Vi verifierar denna metod med syntetiska data och jonakustiska vågor observerade i solvinden. Som en del av det pågående arbetet är vi i färd med att tillämpa denna metod för att identifiera de olika elektrostatiska vågorna och studera utvecklingen av deras egenskaper över en kvasi-vinkelrät bogchock.

Sådana elektrostatiska vågor med hög amplitud kan effektivt växelverka med elektroner när dessa passerar chocken, men det är fortfarande omtvistat hur mycket detta bidrar till upphettning av elektronerna. Två modeller har föreslagits för att besvara detta. Den första betonar adiabatisk växelverkan med DC-fält i chocken för upphettning av elektroner, med sekundära effekter från våg-partikel-växelverkan. Den andra betonar icke-adiabatisk våg-partikel-växelverkan för att förklara upphettning av elektroner när dessa passerar chocken. I artikel V använder vi databasen med chock-passager utvecklad i artikel II för att studera utvecklingen av elektronfördelningsfunktioner när dessa passerar 310 kvasi-vinkelräta chocker genom att använda Liouvilles teorem. Vi finner att mekanismen för elektronupphettning beror på de makroskopiska

chock-parametrarna, nämligen Alfvén-Mach-talet i de Hoffman Teller referenssystemet. Vi finner också att för chocker med främst icke-adiabatisk elektron-dynamik, så är upphettningsmekanismen konsistent med mekanismen för stokastisk drift-acceleration (stochastic shock drift acceleration, SSDA).

9. Summary in Arabic

عندما يتحرّك جسم ما في سائل ما، كالكرة في الهواء مثلًا، تتشكّل أمام هذا الجسم موجات صوتيّة تكون بمثابة إنذار بأنّه ثمّ جسم متحرّك في الهواء. هذه الموجات الصوتيّة تعين الهواء على التحرّك بسلاسة حول الجسم. في حال كانت سرعة هذا الجسم تفوق سرعة الصوت في الهواء، كما حال الرصاصة أو الطائرة النفاثة، فسيسبق هذا الجسم الموجات الصوتيّة، وسيفاجئ الهواء دون تحذير مسبق! وسيُنشئ هذا حالة تُعرف بظاهرة موجة الصدمة . موجة الصدمة هي واجهة رفيعة جدّا، من خلالها تتحوّل طاقة الحركة العالية للجسم إلى طاقة حراريّة. الرّسم 4.1 يمينا، هو صورة عالية الدقّة لموجة الصدمة المتشكّلة حول رصاصة وهي تتحرّك في الهواء.

هذه الظاهرة هي ظاهرة كونيّة لا أرضيّة فقط. بمعنى أنّه يمكننا ملاحظة تشكّلها في أبعاد هذا الكون. أقرب مثال لتلك الظاهرة في الفضاء هو موجة صدمة متشكّلة أمام الكرة الأرضيّة. إنّ الشمس تقذف من مكوّناتها في كلّ ثانية ما يعادل مليار كيلو غرام تقريبًا[1] ، مشكّلة ما يعرف بالرياح الشمسيّة. هذه الرياح الشمسيّة هي في حالة البلازما[2] ، حرارتها جدّا عالية، قد تصل لعشرات الآلاف من الدرجات المئويّة، وتسير بسرعة تفوق سرعة الصوت، قد تصل الى الألف كيلو متر بالثانية. إذا ارتطمت هذه الرياح بغلاف جويّ لكوكب ما أحرقته، كما حصل على المريخ. ولكن للكرة الأرضيّة درع واق، وهو حقلها المغناطيسيّ. عندما ترتطم الرياح الشمسيّة بغلافنا المغناطيسيّ، تراه عائقا، يبطئ من سرعتها وبالتالي ينتج عن ذلك التباطؤ موجة صدمة حول الأرض، خلالها يتحوّل جزء كبير من طاقة الحركة للرياح الشمسيّة لطاقة حراريّة.

[1] ما يوازي وزن مليون سيّارة كل ثانية!

[2] البلازما هي الحالة الرابعة للمادّة بعد الجماد والسوائل والغازات.

العامل الفيزيائي الّذي يسبّب تحوّل طاقة الحركة الى طاقة حراريّة في ظاهرة الموجات الصدميّة الحاصلة ضمن غلافنا الجويّ هو الارتطامات ما بين الذرّات. أمّا في الفضاء، فكثافة البلازما خفيفة جدّا لدرجة أنّ هذه الارتطامات بين الذرّات شبه معدومة. في هذه الحالة ما هي الآليّات الفيزيائيّة التي تساعد على تحويل طاقة الحركة لطاقة حراريّة؟ الجواب على هذا السؤال يكمن في التفاعلات بين جُزيْئات البلازما والتموّجات في الحقلين الكهربائيّ والمغناطيسيّ. تفاصيل هذه التفاعلات ليست معروفة بعد، وهي من الأمور التي لا تزال قيد البحث والدراسة.

في هذه الأطروحة أعمل على المساهمة في الإجابة عن بعض الجزئيّات المتعلّقة بديناميكيّات موجات الصدمة عند غياب الارتطام بين جزيئات البلازما. أقوم بذلك عبر تحليل بيانات مرسلة من مهمّة MMS التابعة لوكالة ناسا. وهي مهمّة استكشاف فضائيّة مؤلّفة من أربعة أقمار اصطناعيّة تدور بتشكيلة هرميّة حول الأرض. هذه الأقمار ترسل لنا قياسات ذات دقّة عالية لأمور مختلفة متعلّقة بحالة البلازما في الفضاء، كالحرارة والكثافة والحقلَين الكهربائيّ والمغناطيسيّ وغيرها.

هذه الأطروحة مبنيّة على خمسة مقالات علميّة محكّمة. ثلاثة منها هدفها تطوير أدوات تحليليّة وقاعدة بيانات تساعد الباحثين على فهم فيزياء موجة الصدمة المتشكّلة حول الكرة الأرضيّة. أمّا المقالَين الباقيين فيتطرّقان إلى الأسئلة العلميّة بشكل مباشر. نستكشف في الأوّل نوعًا معيّنًا من الموجات الكهرومغناطيسيّة يعرف بموجات الصفير الذي يلعب دورًا مهمًّا في ديناميكيّات موجات الصدمة في البلازما في الفضاء، ونحاول فهم آليّة توليد هذا النوع من الموجات. أمّا في المقال الآخر، فإنّنا ندرس الآليّات المختلفة التي تمكّن الإلكترونات من اكتساب طاقتها الحراريّة عندما تمرّ خلال موجات الصدمة.

10. Acknowledgements

بسم الله الرّحمن الرّحيم

In the name of God, the most gracious the most merciful.

I am a scientist, with all the baggage that comes with the trade. I am curious, skeptic and I ask a lot of questions[1]. I also firmly believe that I am where I am because of God's will[2]. He destined that I switch from studying medicine to physics to engineering, and back to physics. He also destined that I do my Ph.D. at the Swedish Institute for Space Physics in Uppsala (IRFU) under the supervision of Yuri and Daniel and with IRFU's wonderful team of scientists and engineers. That is why I start my acknowledgment section by expressing my deep gratitude to God. I am overwhelmed with his blessings and his grace.

The past four and a half years have been a journey of learning and growth. Through that journey, I was not alone. Yuri and Daniel, your guidance and constructive criticism started from day one. I have learned much from your vast knowledge of space physics and space instrument design. Thank you for it all, and I hope that this is nothing but the start of a long-lasting collaboration on many projects to come! Andris, our discussions, even though are not numerous, surely are rich and insightful. I surely looked forward to having them and I look forward to our future discussions. Andrew, thank you for always offering support and guidance when needed. I have enjoyed all of our discussions and collaborations and I surely hope that they don't end with my Ph.D.. I cannot forget to thank Mats for his help at the start of my Ph.D. and for helping with Chapter 8 of the thesis. Also, Anders, Emilya, and Luca thank you for putting up with my numerous questions, and thank you for sharing your vast knowledge of space instrument design and space plasma turbulence.

One of the things I look forward to when I travel or move to a new place is meeting new people. People whose backgrounds and thoughts might be different from mine. For me, this is an eye-opening experience, and an opportunity to learn from our diversity. In that regard, my experience at IRFU did not disappoint! Everyone at IRFU (and KTH) the scientists and engineers have left their impression on me and have provided me with a friendly and welcoming environment that allowed me to feel at home away from home, for that I thank you all. Savvas and Martin, my journey with shocks started

[1] Anyone whom I've taken a course with or attended a conference with can attest to the last point.

[2] In my opinion, the first and second sentences are not incompatible as some might think.

with you guys. I really enjoyed all of our discussions and collaborations and I look forward to future collaborations! Fredrik, Andreas, Konrad, Katerina, Josh, Ida, Jordi, Konstatin, Jack, and all the Ph.D. students and Postdocs at IRFU and KTH, from our frequent discussions[3] to our hikes and outings, I am really happy that I've met you all. Thank you Mengmeng for providing useful comments on my thesis. A special mention has to go to Louis, we have spent four and half years in the same office[4] full of lengthy discussions[5] on science, politics, philosophy, and religion and full of humor(?)[6]. Your love for Python and your distaste of the dayside are remarkable. I hope that the future is full of interesting discussions and collaborations!

As I finalize my Ph.D. Thesis, I cannot forget to thank Ghassan Antar, my Master's thesis supervisor. In your lab, the Laboratory for Plasma and Fluid Mechanics (LPFD) my journey into research started. I have learned a lot from you, thank you for your constant support and guidance. Also, I would not forget to thank Jihad Touma and Leonid Klushin, as I study the nonlinear dynamics and the statistical mechanics of space plasma phenomena, I still reflect on the many deep insights that you shared with us in your classes. Theodore (Teddy) Christidis, the many hours that I spent in your experimental physics labs and the long discussions we had about the physics behind every experiment we built have surely left their mark on me as a scientist. I was saddened to hear of your passing in November of 2022, and more saddened that I was not able to attend your funeral. May your soul rest in peace!

In 2019 I moved $\sim$ 3500 km away from home. It was and still is a great experience full of adventures and challenges that force me to be outside of my comfort zone[7]. Being in such a state requires a solid support system on which I can constantly rely. I am thankful to God for He has blessed me with the unconditional support of my Mom, brothers, sister, and my second family at Al-Amine Mosque in Beirut. Words cannot express how grateful I am to have you all in my life. Thank you Ahmad Balkis and Hani Ramadan for proofreading Chapter 9.

As scientists we are not detached from the world we live in, on the contrary, we are affected by it and we are capable of affecting it. I come from a very turbulent[8] region. Examples of the things that had happened in the past five years alone[9] range from full economic collapses devastating people's livelihood to the largest non-nuclear explosion[10], to the loss of tens of thousands of

[3] Science related or not

[4] From October 2, 2019, to April 1, 2024.

[5] Mostly unfinished!

[6] Mostly dark - sometimes too dark.

[7] Right where I like to be!

[8] Not the kind of turbulence whose structure function can be calculated. Not yet at least...

[9] i.e. the approximate duration of my Ph.D. studies.

[10] I was in Lebanon for this one, and I got to have a first-hand experience of the hydrodynamic version of the phenomena that I study, the shock wave.

innocent lives due to wars[11]. Such turbulence can easily make a person feel helpless and lose the motivation to innovate and to be curious. I myself struggled with the fact that while I live in Sweden, I am safe, following my dreams, working, and studying, while the people who are close to me are constantly in harm's way. The things that got me through this are the values instilled in me growing up in such a place and learning from the resilience and the will to live of the same people who are experiencing the turbulence and their deep faith that things will eventually get better. To the resilient children, women, and men of Lebanon, Palestine, Syria, Sudan, Yemen, and the world, who have faced or are facing unfathomable hardships, thank you for being an inspiration. Your resilience, your will to live, and your will to innovate and explore, have surely inspired me to keep pushing and to strive to be the best version of myself. And I hope, that one day, this turbulence will dissipate, and we can all live safely and follow our dreams[12]!

[11] As of the writing of this thesis, over 30,000 civilians have lost their lives in Gaza, with the toll continuing to rise. Among them, over 25,000 are children and women.

[12] Maybe then, an international space physics conference can be arranged in the region!

Bibliography

Amano, T. et al. (2020). "Observational evidence for stochastic shock drift acceleration of electrons at the Earth's bow shock". In: *Physical review letters* 124.6, p. 065101.

Amano, T. and M. Hoshino (2022). "Theory of electron injection at oblique shock of finite thickness". In: *The Astrophysical Journal* 927.1, p. 132.

Angelopoulos, V. (2009). *The THEMIS mission*. Springer.

Bale, S. et al. (2005). "Quasi-perpendicular shock structure and processes". In: *Space Science Reviews* 118, pp. 161–203.

Balikhin, M. et al. (1998). "A study of the dispersion of the electron distribution in the presence of E and B gradients: Application to electron heating at quasi-perpendicular shocks". In: *Journal of Geophysical Research: Space Physics* 103.A2, pp. 2029–2040.

Balikhin, M. et al. (2005). "Ion sound wave packets at the quasiperpendicular shock front". In: *Geophysical Research Letters* 32.24.

Balikhin, M. et al. (1997a). "Determination of the dispersion of low frequency waves downstream of a quasiperpendicular collisionless shock". In: *Annales Geophysicae*. Vol. 15. 2. Springer Verlag Göttingen, Germany, pp. 143–151.

Balikhin, M. et al. (1997b). "Experimental determination of the dispersion of waves observed upstream of a quasi-perpendicular shock". In: *Geophysical research letters* 24.7, pp. 787–790.

Balogh, A. and R. A. Treumann (2013). *Physics of collisionless shocks: space plasma shock waves*. Springer Science & Business Media.

Baumjohann, W. and R. A. Treumann (2012). "Basic space plasma physics". In.

Berthomier, M. et al. (2000). "Electron-acoustic solitons in an electron-beam plasma system". In: *Physics of Plasmas* 7.7, pp. 2987–2994.

Blasi, P. (2013). "The origin of galactic cosmic rays". In: *A&ARv* 21, 70, p. 70. DOI: 10.1007/s00159-013-0070-7.

Burch, J. et al. (2016). "Magnetospheric multiscale overview and science objectives". In: *Space Science Reviews* 199.1-4, pp. 5–21.

Burgess, D. and M. Scholer (2015). "Collisionless shocks in space plasmas: Structure and accelerated particles". In.

Bykov, A. M. and R. A. Treumann (2011). "Fundamentals of collisionless shocks for astrophysical application, 2. Relativistic shocks". In: *Astronomy and Astrophysics Reviews* 19, 42, p. 42. DOI: 10.1007/s00159-011-0042-8.

Califf, S. and C. M. Cully (2016). “Empirical estimates and theoretical predictions of the shorting factor for the THEMIS double-probe electric field instrument”. In: *Journal of Geophysical Research (Space Physics)* 121.7, pp. 6223–6233. DOI: 10.1002/2016JA022589.

Chen, L.-J. et al. (2018). “Electron bulk acceleration and thermalization at Earth’s quasiperpendicular bow shock”. In: *Physical review letters* 120.22, p. 225101.

Chew, G. F., M. L. Goldberger, and F. Low (1956). “The Boltzmann equation an d the one-fluid hydromagnetic equations in the absence of particle collisions”. In: *Proceedings of the Royal Society of London. Series A. Mathematical and Physical Sciences* 236.1204, pp. 112–118.

De Hoffmann, F. and E. Teller (1950). “Magneto-hydrodynamic shocks”. In: *Physical Review* 80.4, p. 692.

Dimmock, A. P. et al. (2013). “Dispersion of low frequency plasma waves upstream of the quasi-perpendicular terrestrial bow shock”. In: *Annales Geophysicae* 31.8, pp. 1387–1395. DOI: 10.5194/angeo-31-1387-2013.

Edmiston, J. and C. Kennel (1984). “A parametric survey of the first critical Mach number for a fast MHD shock”. In: *Journal of plasma physics* 32.3, pp. 429–441.

Ergun, R. et al. (2016). “The axial double probe and fields signal processing for the MMS mission”. In: *Space Science Reviews* 199.1-4, pp. 167–188.

Eriksson, A. I. (1998). “Spectral analysis”. In: *ISSI Scientific Reports Series* 1, pp. 5–42.

Escoubet, C., R. Schmidt, and M. Goldstein (1997). “Cluster–science and mission overview”. In: *Space Science Reviews* 79.1-2, pp. 11–32.

Fahleson, U. (1967). “Theory of Electric Field Measurements conducted in the Magnetosphere with Electric Probes”. In: *Space Science Reviews* 7.2-3, pp. 238–262. DOI: 10.1007/BF00215600.

Fairfield, D. H. (1969). “Bow shock associated waves observed in the far upstream interplanetary medium”. In: *Journal of Geophysics Research* 74.14, p. 3541. DOI: 10.1029/JA074i014p03541.

Fairfield, D. H. (1974). “Whistler waves observed upstream from collisionless shocks”. In: *Journal of Geophysical Research* 79.10, pp. 1368–1378.

Farris, M., S. Petrinec, and C. Russell (1991). “The thickness of the magnetosheath: Constraints on the polytropic index”. In: *Geophysical Research Letters* 18.10, pp. 1821–1824.

Feldman, W. et al. (1983). “Electron velocity distributions near the Earth’s bow shock”. In: *Journal of Geophysical Research: Space Physics* 88.A1, pp. 96–110.

Galeev, A. A. et al. (1989). “The role of whistler oscillations in the formation of the structure of high Mach number collisionless shock.” In: *Plasma Astrophysics*. Vol. 1, pp. 165–171.

Gershman, D. J. et al. (2015). "The calculation of moment uncertainties from velocity distribution functions with random errors". In: *Journal of Geophysical Research: Space Physics* 120.8, pp. 6633–6645.
Gershman, D. J. et al. (2017). "Spacecraft and instrument photoelectrons measured by the dual electron spectrometers on MMS". In: *Journal of Geophysical Research: Space Physics* 122.11, pp. 11–548.
Gingell, I. et al. (2019). "Observations of magnetic reconnection in the transition region of quasi-parallel shocks". In: *Geophysical Research Letters* 46.3, pp. 1177–1184.
Goodrich, C. and J. Scudder (1984). "The adiabatic energy change of plasma electrons and the frame dependence of the cross-shock potential at collisionless magnetosonic shock waves". In: *Journal of Geophysical Research: Space Physics* 89.A8, pp. 6654–6662.
Goodrich, K. A. et al. (2018). "MMS observations of electrostatic waves in an oblique shock crossing". In: *Journal of Geophysical Research: Space Physics* 123.11, pp. 9430–9442.
Graham, D. B. et al. (2016). "Electrostatic solitary waves and electrostatic waves at the magnetopause". In: *Journal of Geophysical Research: Space Physics* 121.4, pp. 3069–3092.
Gurnett, D. A. (1998). "Principles of space plasma wave instrument design". In: *Geophysical Monograph-American Geophysical Union* 103, pp. 121–136.
Hanson, E. et al. (2020). "Shock Drift Acceleration of Ions in an Interplanetary Shock Observed by MMS". In: *The Astrophysical Journal Letters* 891.1, p. L26.
Harten, R. and K. Clark (1995). "The design features of the GGS wind and polar spacecraft". In: *Space Science Reviews* 71.1-4, pp. 23–40.
Hartley, D. et al. (2016). "Using the cold plasma dispersion relation and whistler mode waves to quantify the antenna sheath impedance of the Van Allen Probes EFW instrument". In: *Journal of Geophysical Research: Space Physics* 121.5, pp. 4590–4606.
Harvey, C. C. (1998). "Spatial gradients and the volumetric tensor". In: *ISSI scientific reports series* 1, pp. 307–322.
Hull, A. J. et al. (2012). "Multiscale whistler waves within Earth's perpendicular bow shock". In: *Journal of Geophysical Research (Space Physics)* 117.A12, A12104, A12104. DOI: 10.1029/2012JA017870.
Hull, A. et al. (2000). "Electron temperature and de Hoffmann-Teller potential change across the Earth's bow shock: New results from ISEE 1". In: *Journal of Geophysical Research: Space Physics* 105.A9, pp. 20957–20971.
Hull, A. J. et al. (2020). "MMS observations of intense whistler waves within Earth's supercritical bow shock: Source mechanism and impact on shock structure and plasma transport". In: *Journal of Geophysical Research: Space Physics* 125.7, e2019JA027290.

Johlander, A. et al. (2016). “Rippled quasiperpendicular shock observed by the magnetospheric multiscale spacecraft”. In: *Physical Review Letters* 117.16, p. 165101.
Johlander, A. et al. (2021). “Ion acceleration efficiency at the Earth’s bow shock: observations and simulation results”. In: *The Astrophysical Journal* 914.2, p. 82.
Johlander, A. et al. (2023). “Electron heating scales in collisionless shocks measured by mms”. In: *Geophysical Research Letters* 50.5, e2022GL100400.
Johnstone, A. et al. (1997). “PEACE: A plasma electron and current experiment”. In: *The Cluster and Phoenix Missions*, pp. 351–398.
Kamaletdinov, S. R., I. Y. Vasko, and A. V. Artemyev (2024). “Nonlinear electron scattering by electrostatic waves in collisionless shocks”. In: *Journal of Plasma Physics* 90.2, p. 905900201.
Kamaletdinov, S. et al. (2022). “Quantifying electron scattering by electrostatic solitary waves in the Earth’s bow shock”. In: *Physics of Plasmas* 29.8.
Katou, T. and T. Amano (2019). “Theory of stochastic shock drift acceleration for electrons in the shock transition region”. In: *The Astrophysical Journal* 874.2, p. 119.
Kennel, C., J. Edmiston, and T. Hada (1985). “A quarter century of collisionless shock research”. In: *Collisionless shocks in the heliosphere: A tutorial review* 34, pp. 1–36.
King, J. and N. Papitashvili (2005). “Solar wind spatial scales in and comparisons of hourly Wind and ACE plasma and magnetic field data”. In: *Journal of Geophysical Research: Space Physics* 110.A2.
Krasnoselskikh, V. (1985). “Nonlinear motions of a plasma across a magnetic field”. In: *Sov. Phys. JETP* 62, p. 282.
Krasnoselskikh, V. V. et al. (2002). “Nonstationarity of strong collisionless quasiperpendicular shocks: Theory and full particle numerical simulations”. In: *Physics of Plasmas* 9.4, pp. 1192–1209. DOI: 10.1063/1.1457465.
Krasnoselskikh, V. et al. (2013). “The dynamic quasiperpendicular shock: Cluster discoveries”. In: *Space Science Reviews* 178, pp. 535–598.
Krasnoselskikh, V. et al. (1991). “On the nature of low frequency turbulence in the foot of strong quasi-perpendicular shocks”. In: *Advances in Space Research* 11.9, pp. 15–18.
Krauss-Varban, D., D. Burgess, and C. Wu (1989). “Electron acceleration at nearly perpendicular collisionless shocks, 1, One-dimensional simulations without electron scale fluctuations”. In: *Journal of Geophysical Research: Space Physics* 94.A11, pp. 15089–15098.
Kurtmullaev, R. K. et al. (1965). “Excitation of strong collisionless shock waves in a plasma”. In: *Journal of Applied Mechanics and Technical Physics* 6.2, pp. 68–73.
LaBelle, J. and P. Kintner (1989). “The measurement of wavelength in space plasmas”. In: *Reviews of Geophysics* 27.4, pp. 495–518.

Lalti, A. et al. (2022a). “A Database of MMS Bow Shock Crossings Compiled Using Machine Learning”. In: *Journal of Geophysical Research: Space Physics* 127.8, e2022JA030454.

Lalti, A., Y. V. Khotyaintsev, and D. B. Graham (2023). “Short-Wavelength Electrostatic Wave Measurement Using MMS Spacecraft”. In: *Journal of Geophysical Research (Space Physics)* 128.4, e2022JA031150, e2022JA031150. DOI: 10.1029/2022JA031150.

Lalti, A. et al. (2022b). “Whistler Waves in the Foot of Quasi-Perpendicular Supercritical Shocks”. In: *Journal of Geophysical Research: Space Physics* 127.5, e2021JA029969.

Le Contel, O. et al. (2016). “The search-coil magnetometer for MMS”. In: *Space Science Reviews* 199.1-4, pp. 257–282.

Lefebvre, B. et al. (2007). “Electron dynamics and cross-shock potential at the quasi-perpendicular Earth’s bow shock”. In: *Journal of Geophysical Research: Space Physics* 112.A9.

Leroy, M. et al. (1982). “The structure of perpendicular bow shocks”. In: *Journal of Geophysical Research: Space Physics* 87.A7, pp. 5081–5094.

Li, H., C. Wang, and J. Richardson (2008). “Properties of the termination shock observed by Voyager 2”. In: *Geophysical research letters* 35.19.

Lindqvist, P.-A. et al. (2016). “The spin-plane double probe electric field instrument for MMS”. In: *Space Science Reviews* 199.1-4, pp. 137–165.

Liu, T. Z., V. Angelopoulos, and S. Lu (2019). “Relativistic electrons generated at Earth’s quasi-parallel bow shock”. In: *Science advances* 5.7, eaaw1368.

Lowe, R. and D. Burgess (2003). “The properties and causes of rippling in quasi-perpendicular collisionless shock fronts”. In: *Annales Geophysicae*. Vol. 21. 3. Copernicus Publications Göttingen, Germany, pp. 671–679.

Mach, E. (1898). *Popular scientific lectures*. 21. Open Court Publishing Company.

Madanian, H. et al. (2021). “The Dynamics of a High Mach Number Quasi-perpendicular Shock: MMS Observations”. In: *The Astrophysical Journal* 908.1, p. 40.

Marshall, W. (1955). “The structure of magneto-hydrodynamic shock waves”. In: *Proceedings of the Royal Society of London. Series A. Mathematical and Physical Sciences* 233.1194, pp. 367–376.

Masters, A. et al. (2011). “Electron heating at Saturn’s bow shock”. In: *Journal of Geophysical Research: Space Physics* 116.A10.

Matsukiyo, S. and M. Scholer (2006). “On microinstabilities in the foot of high Mach number perpendicular shocks”. In: *Journal of Geophysical Research: Space Physics* 111.A6.

Maynard, N. C. (1998). “Electric field measurements in moderate to high density space plasmas with passive double probes”. In: *GEOPHYSICAL MONOGRAPH-AMERICAN GEOPHYSICAL UNION* 103, pp. 13–28.

McFadden, J. et al. (2008). “The THEMIS ESA plasma instrument and in-flight calibration”. In: *Space Science Reviews* 141.1, pp. 277–302.

Montgomery, D. C. and D. A. Tidman (1964). “Plasma kinetic theory”. In: *McGraw-Hill Advanced Physics Monograph Series*.
Mozer, F. (1973). “Analyses of techniques for measuring DC and AC electric fields in the magnetosphere”. In: *Space Science Reviews* 14.2, pp. 272–313.
Mozer, F. (2016). “DC and low-frequency double probe electric field measurements in space”. In: *Journal of Geophysical Research: Space Physics* 121.11, pp. 10–942.
Müller, D. et al. (2020). “The solar orbiter mission-science overview”. In: *Astronomy & Astrophysics* 642, A1.
Muschietti, L. and B. Lembège (2017). “Two-stream instabilities from the lower-hybrid frequency to the electron cyclotron frequency: application to the front of quasi-perpendicular shocks”. In: *Annales Geophysicae* 35.5, pp. 1093–1112. DOI: 10.5194/angeo-35-1093-2017.
Ness, N. F., C. S. Scearce, and J. B. Seek (1964). “Initial results of the Imp 1 magnetic field experiment”. In: *Journal of Geophysical Research* 69.17, pp. 3531–3569.
Oka, M. et al. (2017). “Electron scattering by high-frequency whistler waves at earth’s bow shock”. In: *The Astrophysical Journal Letters* 842.2, p. L11.
Olshevsky, V. et al. (2021). “Automated classification of plasma regions using 3D particle energy distributions”. In: *Journal of Geophysical Research: Space Physics* 126.10, e2021JA029620.
Onsager, T. and R. Holzworth (1990). “Measurement of the electron beam mode in Earth’s foreshock”. In: *Journal of Geophysical Research: Space Physics* 95.A4, pp. 4175–4186.
Pedersen, A., F. Mozer, and G. Gustafsson (1998). “Electric field measurements in a tenuous plasma with spherical double probes”. In: *Geophysical Monograph-American Geophysical Union* 103, pp. 1–12.
Pollock, C. et al. (2016). “Fast plasma investigation for magnetospheric multiscale”. In: *Space Science Reviews* 199.1-4, pp. 331–406.
Robert, P. et al. (1998). “Accuracy of current density determination”. In: *Analysis methods for multi-spacecraft data* 398, pp. 395–418.
Russell, C. et al. (2016). “The magnetospheric multiscale magnetometers”. In: *Space Science Reviews* 199.1-4, pp. 189–256.
Sagdeev, R. (1966). “Cooperative phenomena and shock waves in collisionless plasmas”. In: *Reviews of plasma physics* 4, p. 23.
Santolík, O., M. Parrot, and F. Lefeuvre (2003). “Singular value decomposition methods for wave propagation analysis”. In: *Radio Science* 38.1. DOI: https://doi.org/10.1029/2000RS002523.
Savoini, P. and B. Lembege (1994). “Electron dynamics in two-and one-dimensional oblique supercritical collisionless magnetosonic shocks”. In: *Journal of Geophysical Research: Space Physics* 99.A4, pp. 6609–6635.
Saxena, R., S. Bale, and T. Horbury (2005). “Wavelength and decay length of density overshoot structure in supercritical, collisionless bow shocks”. In: *Physics of plasmas* 12.5.

Schwartz, S. J. (2014). “Comment on “Electron demagnetization and heating in quasi-perpendicular shocks” by Mozer and Sundkvist”. In: *Journal of Geophysical Research: Space Physics* 119.3, pp. 1507–1512.

Schwartz, S. J. et al. (1988). “Electron heating and the potential jump across fast mode shocks”. In: *Journal of Geophysical Research: Space Physics* 93.A11, pp. 12923–12931.

Scudder, J. D. et al. (1986). “The resolved layer of a collisionless, high β, supercritical, quasi-perpendicular shock wave, 3. Vlasov electrodynamics”. In: *Journal of Geophysical Research* 91.A10, pp. 11075–11098. DOI: 10.1029/JA091iA10p11075.

Scudder, J. D. (1995). “A review of the physics of electron heating at collisionless shocks”. In: *Advances in Space Research* 15.8-9, pp. 181–223.

See, V., R. Cameron, and S. Schwartz (2013). “Non-adiabatic electron behaviour due to short-scale electric field structures at collisionless shock waves”. In: *Annales Geophysicae*. Vol. 31. 4. Copernicus Publications Göttingen, Germany, pp. 639–646.

Shi, X. et al. (2023a). “Electron resonant interaction with whistler-mode waves around the Earth’s bow shock I: The probabilistic approach”. In: *Physics of Plasmas* 30.12.

Shi, X. et al. (2023b). “Intense Whistler-mode Waves at Foreshock Transients: Characteristics and Regimes of Wave- Particle Resonant Interaction”. In: *The Astrophysical Journal* 944.2, p. 193.

Sonnerup, B. U. and M. Scheible (1998). “Minimum and maximum variance analysis”. In: *Analysis methods for multi-spacecraft data* 1, pp. 185–220.

Steinvall, K., Y. V. Khotyaintsev, and D. B. Graham (2022). “On the applicability of single-spacecraft interferometry methods using electric field probes”. In: *Journal of Geophysical Research: Space Physics* 127.3, e2021JA030143.

Stone, E. C. et al. (1998). “The advanced composition explorer”. In: *Space Science Reviews* 86, pp. 1–22.

Sulaiman, A., A. Masters, and M. Dougherty (2016). “Characterization of Saturn’s bow shock: Magnetic field observations of quasi-perpendicular shocks”. In: *Journal of Geophysical Research: Space Physics* 121.5, pp. 4425–4434.

Swanson, D. G. (2003). *Plasma waves*. CRC Press.

Tidman, D. A. and N. A. Krall (1971). *Shock waves in collisionless plasmas*.

Tokar, R. L., D. A. Gurnett, and W. C. Feldman (1984). “Whistler mode turbulence generated by electron beams in earth’s bow shock”. In: *Journal of Geophysical Research* 89.A1, pp. 105–114. DOI: 10.1029/JA089iA01p00105.

Torbert, R. et al. (2016). “The FIELDS instrument suite on MMS: Scientific objectives, measurements, and data products”. In: *Space Science Reviews* 199.1-4, pp. 105–135.

Tsurutani, B. T. and P. Rodriguez (1981). “Upstream waves and particles: An overview of ISEE results”. In: *Journal of Geophysical Research: Space Physics* 86.A6, pp. 4317–4324.

Turner, D. et al. (2013). “First observations of foreshock bubbles upstream of Earth’s bow shock: Characteristics and comparisons to HFAs”. In: *Journal of Geophysical Research: Space Physics* 118.4, pp. 1552–1570.
Vasko, I. Y. et al. (2020). “On the nature and origin of bipolar electrostatic structures in the Earth’s bow shock”. In: *Frontiers in Physics* 8, p. 156.
Vasko, I. et al. (2018). “Solitary waves across supercritical quasi-perpendicular shocks”. In: *Geophysical Research Letters* 45.12, pp. 5809–5817.
Vasko, I. et al. (2022). “Ion-Acoustic Waves in a Quasi-Perpendicular Earth’s Bow Shock”. In: *Geophysical Research Letters* 49.11, e2022GL098640.
Wang, R. et al. (2020). “Electrostatic turbulence and Debye-scale structures in collisionless shocks”. In: *The Astrophysical Journal Letters* 889.1, p. L9.
Wilson III, L. B. et al. (2012). “Observations of electromagnetic whistler precursors at supercritical interplanetary shocks”. In: *Geophysics Research Letters* 39.8, L08109, p. L08109. DOI: 10.1029/2012GL051581.
Wilson III, L. B. et al. (2014a). “Quantified energy dissipation rates in the terrestrial bow shock: 1. Analysis techniques and methodology”. In: *Journal of Geophysical Research (Space Physics)* 119.8, pp. 6455–6474. DOI: 10.1002/2014JA019929.
Wilson III, L. B. et al. (2014b). “Quantified energy dissipation rates in the terrestrial bow shock: 2. Waves and dissipation”. In: *Journal of Geophysical Research (Space Physics)* 119.8, pp. 6475–6495. DOI: 10.1002/2014JA019930.
Wilson III, L. B. (2016). “Low frequency waves at and upstream of collisionless shocks”. In: *Washington DC American Geophysical Union Geophysical Monograph Series* 216, pp. 269–291.
Wilson III, L. B. et al. (2009). “Low-frequency whistler waves and shocklets observed at quasi-perpendicular interplanetary shocks”. In: *Journal of Geophysical Research: Space Physics* 114.A10.
Wilson III, L. B. et al. (2013). “Electromagnetic waves and electron anisotropies downstream of supercritical interplanetary shocks”. In: *Journal of Geophysical Research: Space Physics* 118.1, pp. 5–16.
Wilson III, L. B. et al. (2016). “Relativistic electrons produced by foreshock disturbances observed upstream of Earth’s bow shock”. In: *Physical review letters* 117.21, p. 215101.
Wilson III, L. B. et al. (2019). “Electron energy partition across interplanetary shocks. I. Methodology and data product”. In: *The Astrophysical Journal Supplement Series* 243.1, p. 8.
Wilson III, L. B. et al. (2021). *A quarter century of wind spacecraft discoveries*.
Wu, C. et al. (1983). “A kinetic cross-field streaming instability”. In: *The Physics of Fluids* 26.5, pp. 1259–1267.
Wu, C. et al. (1984). “Microinstabilities associated with a high Mach number, perpendicular bow shock”. In: *Space science reviews* 37, pp. 63–109.

Xie, H.-S. (2019). “BO: A unified tool for plasma waves and instabilities analysis”. In: *Computer Physics Communications* 244, pp. 343–371. DOI: https://doi.org/10.1016/j.cpc.2019.06.014.

Yang, Z. et al. (2020). “MMS direct observations of kinetic-scale shock self-reformation”. In: *The Astrophysical Journal Letters* 901.1, p. L6.

Zhang, T. et al. (2008). “Initial Venus Express magnetic field observations of the magnetic barrier at solar minimum”. In: *Planetary and Space Science* 56.6, pp. 790–795.

Acta Universitatis Upsaliensis

Digital Comprehensive Summaries of Uppsala Dissertations from the Faculty of Science and Technology 2388

Editor: The Dean of the Faculty of Science and Technology

A doctoral dissertation from the Faculty of Science and Technology, Uppsala University, is usually a summary of a number of papers. A few copies of the complete dissertation are kept at major Swedish research libraries, while the summary alone is distributed internationally through the series Digital Comprehensive Summaries of Uppsala Dissertations from the Faculty of Science and Technology. (Prior to January, 2005, the series was published under the title "Comprehensive Summaries of Uppsala Dissertations from the Faculty of Science and Technology".)

Distribution: publications.uu.se
urn:nbn:se:uu:diva-526127

ACTA UNIVERSITATIS
UPSALIENSIS
2024